

Optical nanoresonators

V V Klimov

DOI: <https://doi.org/10.3367/UFNe.2022.02.039153>

Contents

1. Introduction	263
2. General approaches to describing optical nanoresonator properties	264
2.1 Closed resonator eigenmodes; 2.2 Open nanoresonator eigenmodes; 2.3 Anapole current distributions and eigenmodes; 2.4 Symmetry properties of modes in optical nanoresonators; 2.5 Perturbation theory methods for describing the properties of optical nanoresonators; 2.6 Numerical methods for describing the properties of optical nanoresonators	
3. Modes in plasmonic nanoresonators	269
3.1 Optical properties of spherical plasmonic resonators; 3.2 Optical properties of spheroidal and ellipsoidal plasmonic resonators; 3.3 Optical properties of clusters of plasmonic resonators	
4. Modes in dielectric nanoresonators	273
4.1 Spherical dielectric nanoresonators; 4.2 Spheroidal nanoresonators; 4.3 Dielectric nanoresonators of more complex shapes	
5. Modes in nanoresonators made of metamaterials	280
5.1 Modes in a sphere with a negative refractive index; 5.2 Modes in a chiral sphere; 5.3 Modes in a sphere made of a hyperbolic metamaterial	
6. Examples of possible applications of optical nanoresonators	284
7. Conclusion	284
References	285

Abstract. The review presents an analysis and generalization of classical and most modern approaches to the description and development of the principles of operation of open optical nanoresonators, that is, resonators, all sizes of which are smaller than the resonant wavelength of radiation in vacuum. Particular attention is paid to the physics of such phenomena as bound states in a continuum, anapole states, supercavity modes, and perfect nonradiating modes with extremely high quality factors and localizations of electromagnetic fields. An analysis of the optical properties of natural oscillations in nanoresonators made of metamaterials is also presented in the review. The effects considered in this review, besides being of fundamental import, can also find applications in the development of optical nanoantennas, nanolasers, biosensors, photovoltaic devices, and nonlinear nanophotonics.

Keywords: nanoresonators, quasi-normal modes, perfect nonradiating modes, supercavity modes, anapole states, bound states in a continuum, Platonic solids, quality factor, nanoantennas, nanolasers, metamaterials, Mie resonances, plasmon resonances, biosensors

V V Klimov

Lebedev Physical Institute, Russian Academy of Sciences,
Leninskii prosp. 53, 119991 Moscow, Russian Federation
E-mail: klimov256@gmail.com

Received 10 August 2021, revised 17 January 2022
Uspekhi Fizicheskikh Nauk 193 (3) 279–304 (2023)
Translated by A V Sharonova

1. Introduction

For modern optical devices, the localization of light in volumes of any size smaller than the wavelength in vacuum, that is, in nanoresonators, becomes critically important. The localization is extremely important for such modern applications of nano-optics as lasers and spasers, optical nanoantennas, metasurfaces, chemical and biological sensors, optical computers, filters, switches, detectors, and optical memory elements. The compactness of these devices allows one to integrate them into optical microcircuits, and that is extremely important, since the miniaturization process in the production of electronic microcircuits has almost reached the theoretical limit. In this regard, the resonant optical properties of plasmonic nanoparticles [1–6] and dielectric nanoparticles with a high refractive index [7–25] are currently being actively studied. Figure 1 shows examples of optical nanoresonators.

The physics of optical phenomena in such nanostructures is very complex and leads to many interesting applications, such as nano-antennas [5, 6, 8–14], plasmonic [2, 4] and nonplasmon nanolasers [22, 25, 26], and nonlinear nanophotonics [17, 21, 27, 28]. As in any other field of physics, here, all effects are associated with the existence of certain modes of natural oscillations in nanoparticles.

For applications, eigenmodes with strong field localization and low radiation losses are of particular interest. Modes of this kind have recently attracted the closest attention of leading scientific groups, which have discovered several types of weakly radiating systems: bound states in a continuum [27–30], anapole current distribu-

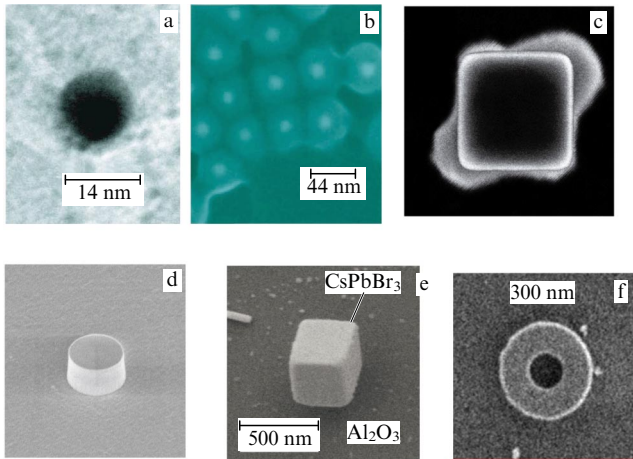


Figure 1. (a) Transmission electron microscope image of a gold spherical nanoresonator with a diameter of 14 nm [2]. (b) Scanning electron microscope (SEM) image of a spaser based on the resonator shown in (a) [2]. (c) SEM image of a gold single-crystal nanoresonator with an edge of 100 nm with opposite edges covered by a polymer doped with CdSe/CdS/Zn (core/shell/shell) colloidal quantum dots [3]. (d) SEM image of a cylindrical AlGaAs nanoresonator (refractive index $n = 3.4$) 635 nm high and 930 nm in diameter on a quartz substrate [20, 21]. (e) SEM image of a CsPbBr₃ cubic nanoresonator with an edge of 310 nm on a sapphire substrate [22]. (f) SEM image of an Si ring resonator with outer and inner diameters of 800 and 300 nm, respectively, and a thickness of 80 nm [23].

tions [19, 31–36], supercavity modes [25, 37, 38], and perfect nonradiating modes [39–41].

Due to radiation losses, intermode interference, and amplification of both electric and magnetic fields, the physics of high- Q modes in nanoresonators is very complex. In particular, the fields of usual quasi-normal modes increase without limit at infinity. In view of the exceptional importance of open nanoresonators, a number of approaches are being intensively developed at present to describe them and to create new nanodevices based on them.

These approaches are not well known to a wide range of physicists working in the field of nano-optics and nanoplasmonics and their applications. Therefore, the purpose of this review is to analyze and generalize the most modern approaches to the description and development of open nanoresonators, that is, resonators of a size smaller than the wavelength of radiation in vacuum. The large flow of work in this area has led to the fact that their character is mainly phenomenological and/or purely computational. Therefore, one of the important objectives of the review is to present the situation from a single, well-defined point of view. In doing so, we restrict ourselves to the case of resonators of simple shapes with high symmetry, allowing a more or less accurate description of their resonant properties. The properties of asymmetric resonators are also very interesting (see, for example, [42]), but they critically (even chaotically) depend on small shape variations, and their study deserves a separate review.

Section 2 of the review will present general approaches to the description of optical nanoresonators. Here, various definitions and methods for finding their eigenmodes and eigenvalues will be analyzed. Particular attention will be paid to studies where alternative methods for describing eigenmodes are developed that do not have the disadvantages inherent in the standard description. This section will also

analyze the underlying software for finding eigenmodes and eigenvalues. Section 3 will present studies of eigen oscillations in plasmonic nanoresonators of various shapes (spheres, spheroids, ellipsoids, Platonic solids, clusters of nanoparticles). In Section 4, we will consider investigations of eigen oscillations in dielectric nanoresonators of various shapes (spheres, spheroids, cylinders). Section 5 will analyze studies of eigen oscillations in nanoresonators made from chiral and hyperbolic metamaterials, as well as from metamaterials with a negative refractive index. Section 6 of the review will present examples of the use of nanoresonators for nanolasers, biosensors and nonlinear optical devices, and optical and quantum computers. Throughout the review, it is assumed that the dependence of fields on time has the form $\exp(-i\omega t)$.

2. General approaches to describing optical nanoresonator properties

2.1 Closed resonator eigenmodes

Describing the properties of electromagnetic waves in resonators is a classical problem of mathematics and the theory of electromagnetic waves (see, for example, [43–45]). In classical studies, the main focus is on closed resonators, that is, resonators without radiation losses.

Natural oscillations of such resonators are described by Maxwell equations with the condition of perfect conductivity of walls:

$$\nabla \times \nabla \times \mathbf{E}_n = k_{0,n}^2 \varepsilon \mathbf{E}_n, \quad (1)$$

$$\mathbf{E}_{n,\tan}|_S = 0.$$

For resonators without internal losses, $\text{Im} \varepsilon = 0$, the eigenfrequencies of system (1) $\omega_n = ck_{0,n}$ are real numbers, and the modes for different frequencies are orthogonal. This makes it possible to solve all practically interesting problems concerning the excitation of such resonators and the interaction of waves in them. Losses in the walls of waveguides can be considered using perturbation theory [43]. The theory of closed resonators is the basis for considering any resonators.

2.2 Open nanoresonator eigenmodes

In addition to closed resonators, both in microwave technology and in modern applications of nano-optics, open nanoresonators, where natural oscillations lead to the emission of energy and the associated damping of oscillations, are of great importance [46].

2.2.1 What are open nanoresonator modes? The concept of a ‘resonator mode’ seems to be well known, and this is true for closed resonators that are used in microwave technology. However, when applied to optical nanoresonators based on nanoparticles, the concept of ‘resonator mode’ becomes far from trivial, since they are open systems [46], and oscillations in the resonator volume interact with a continuum of free space modes. So, the definition of modes in open resonators as solutions of Maxwell’s equations without sources becomes incomplete, since for open resonators it is also necessary to specify the character of the behavior of fields at infinity, which can be very different both formally and when considering specific problems. Setting certain conditions at infinity imposes restrictions on the choice of spectral parameters that can be eigenvalues of the resonator modes.

In any case, the main characteristics of the resonators are the resonant frequencies ω_n and the quality factors Q_n , according to definition [43], equal to the ratio of the energy stored in the n th mode of the resonator $W_{n,\text{stored}}$ to the power $P_{n,\text{rad}}$ radiated by the same mode:

$$Q_n = \frac{\omega_n W_{n,\text{stored}}}{P_{n,\text{rad}}} \quad (2)$$

This definition assumes that the eigenmodes have already been found in one way or another. However, in practice, in the case of open resonators, it is often difficult to find natural oscillations directly, and in this case the concept of a generalized quality factor turns out to be extremely useful, being valid at any frequency [47–49], in contrast to (2):

$$Q(\omega) = \frac{\omega W_{\text{stored}}(\omega)}{P_{\text{rad}}(\omega)} \quad (3)$$

In (3), the stored energy $W_{\text{stored}}(\omega)$ and the radiated power $P_{\text{rad}}(\omega)$ can be found by solving the scattering problem at an arbitrary frequency. At frequencies corresponding to those of natural oscillations, this expression naturally coincides with the usual definition (2). However, the concept of a generalized Q -factor turns out to be very useful in nontrivial cases when the stored energy does not have resonant properties and radiation losses have minima (see Sections 4.1.4, 4.2.2, 4.3.3, 5.1). Calculations of the energy stored in the resonator, W_{stored} , for open resonators can be carried out in various ways [50]. In this review, by stored energy we mean, as usual [43], the positive energy that is concentrated inside the resonator.

2.2.2 Frequency as mode eigenvalue. In the case of open resonators — and this is the case that is the subject of this review — it is usually assumed (as in the theory of closed resonators) that the eigenvalue is the oscillation frequency, and the modes are defined as solutions of the Maxwell equation

$$\nabla \times \nabla \times \mathbf{E}_n = k_{0,n}^2 \varepsilon \mathbf{E}_n \quad \text{inside nanoresonator,} \quad (4)$$

$$\nabla \times \nabla \times \mathbf{E}_n = k_{0,n}^2 \mathbf{E}_n \quad \text{outside nanoresonator,}$$

where ε is the permittivity of the nanoresonator, with Sommerfeld radiation conditions at infinity [51]:

$$\mathbf{E}(r, \theta, \varphi) \xrightarrow{r \rightarrow \infty} \frac{\exp(ik_{0,n}r)}{r} \mathbf{F}(\theta, \varphi). \quad (5)$$

In (4), ε stands for resonator permittivity.

However, such a formulation of the problem is contradictory, since, due to radiation and the energy conservation law, it follows that the eigenfrequencies Ω_n are complex numbers, $\Omega_n = \omega_n - i\Gamma_n/2$, leading, in turn, to an unlimited increase in the mode fields at infinity

$$E_n(\mathbf{r}) \sim \frac{\exp(i\Omega_n r/c)}{r} = \frac{\exp(i\omega_n r/c) \exp(\Gamma_n r/2c)}{r} \xrightarrow{r \rightarrow \infty} \infty. \quad (6)$$

L A Weinshtein drew attention for the first time to this fact [46]: “This increase is an inevitable consequence of the exponential damping of the field as $t \rightarrow \infty$. Indeed, since at $R \rightarrow \infty$ the field of each natural oscillation has the character of a spherical wave going to infinity at the speed of light, then,

for example, at $t = 0$, the field at a large distance R is due to a wave emitted by a sphere at $t = -R/c$ when the oscillation amplitude in it was much greater than at $t = 0$, due to which this field is exponentially large. The above considerations are very general and allow us to assert that the exponential increase in the field of eigen oscillations at $R \rightarrow \infty \dots$ takes place for all open resonators (three-dimensional).”

Eigenmodes of open systems are also known as decaying states, leaky modes, quasi-modes, or quasi-normal modes.

The main problem in the description and computer simulation of quasi-modes or modes of open resonators is to determine how they can be normalized. Since these modes increase at infinity, the usual normalization procedures do not work, and nonstandard solutions are needed.

A number of approaches to the normalization of quasi-modes have been proposed in [46, 52–59]. In [58], the eigenfunctions of spherical resonators, which are solutions of the Maxwell equations without sources,

$$\nabla \times \nabla \times \mathbf{E}_n - k_{0,n}^2 \varepsilon(|\mathbf{r}|) \mathbf{E}_n = 0, \quad (7)$$

are proposed to be normalized using the relation

$$\int_V d\mathbf{r} \varepsilon(|\mathbf{r}|) \mathbf{E}_n^2(\mathbf{r}) + \frac{1}{2k_n^2} \int_S dS \left(\mathbf{E}_n \frac{\partial \mathbf{E}_n}{\partial r} + r \mathbf{E}_n \frac{\partial^2 \mathbf{E}_n}{\partial r^2} - r \left(\frac{\partial \mathbf{E}_n}{\partial r} \right)^2 \right) = 1, \quad (8)$$

where the integration is carried out over the spherical resonator volume V and over the surface of the large sphere S surrounding the volume V . In (8), the volume and surface integrals, taken separately, diverge, but their sum remains finite.

To find the eigenfrequencies and Q -factors of nanoresonators, one can use the method of integral equations (see, for example, [60–63]), where, apparently, there are no problems with field divergences at infinity, which arise when solving partial differential equations (4). However, the low prevalence of this method indicates the complexity of its application.

2.2.3 Permittivity as mode eigenvalue. More reliable and unambiguous results are obtained if we use not the frequency (as is usually done), but the permittivity ε_n of the nanoresonator [1, 64, 65] as an eigenvalue. In this case, the eigenfunctions satisfy the Maxwell equations

$$\nabla \times \nabla \times \mathbf{E}_n = k_0^2 \varepsilon_n \mathbf{E}_n \quad \text{inside resonator,} \quad (9)$$

$$\nabla \times \nabla \times \mathbf{E}_n = k_0^2 \mathbf{E}_n \quad \text{outside resonator,}$$

and the Sommerfeld conditions (5) at infinity.

In (9), $\omega = k_0 c$ is the real frequency, and the permittivity eigenvalue ε_n is a complex number. It can be shown [1, 64, 65] that its imaginary part is negative, $\text{Im } \varepsilon_n < 0$, and this can be interpreted as an amplifying medium that compensates radiation losses. It is this circumstance that causes the fields of eigenfunctions \mathbf{E}_n to decrease at infinity. In addition, the smallest eigenvalues ε_n have a negative real part, making this method especially useful for describing the properties of plasmonic nanoresonators. We emphasize once again that in system (9) the actual material properties of the resonator do not appear.

The expansion of solutions of Maxwell’s equations in terms of eigenmodes for an arbitrary excitation field \mathbf{E}^0 in the

framework of the ‘ ε -method’ has a simple form:

$$\mathbf{E} = \mathbf{E}^0 + \sum_n \mathbf{E}_n \frac{\varepsilon(\omega) - 1}{\varepsilon_n - \varepsilon(\omega)} \frac{\int_V \mathbf{E}_n \mathbf{E}^0 dV}{\int_V \mathbf{E}_n^2 dV}, \quad (10)$$

where $\varepsilon(\omega)$ describes the frequency dependence of the permittivity of the resonator’s specific material, and the integration is carried out over the volume of the resonator V .

It follows from the form of this solution that $\varepsilon(\omega)$ enters into (10) in a rather simple way, making it easy to carry out calculations for nanoresonators of the same shape, but made of different materials. This is very important when optimizing certain nanodevices.

The most important feature of solution (10) is the presence of the resonance factor $(\varepsilon_n - \varepsilon(\omega))$ in the denominator. At frequencies ω_n such that $\varepsilon_n - \varepsilon(\omega_n) \approx 0$, the resonance occurs in the system, and only one term becomes significant in the solution:

$$\mathbf{E} \approx \mathbf{E}^0 + \mathbf{E}_n \frac{\varepsilon(\omega) - 1}{\varepsilon_n - \varepsilon(\omega)} \frac{\int_V \mathbf{E}_n \mathbf{E}^0 dV}{\int_V \mathbf{E}_n^2 dV}. \quad (11)$$

In this case, one can speak of excitation at a frequency ω_n of a localized mode with a spatial structure described by the mode field \mathbf{E}_n , which does not depend at all on a particular material.

The width of the resonance as a function of frequency essentially depends on the imaginary parts of ε_n and $\varepsilon(\omega)$. It is very important to note that the imaginary parts of ε_n and $\varepsilon(\omega)$ always have different signs, and therefore the resonance width of (11) is determined by the sum of their moduli. As will be shown below, in the case of nanoresonators, the imaginary part of $\varepsilon_n'' \sim (ka)^3$ becomes very small. In this case, the width of the resonance is mainly determined by the losses inside the nanoparticles, that is, by the imaginary part of $\varepsilon(\omega)$. In those cases where the imaginary part is small, it becomes necessary to take the imaginary part of ε_n into account, and a number of interesting effects arise in this case [66].

Thus, within the framework of the ‘ ε -method,’ plasmon oscillations arise naturally as a result of solving the spectral problem where the eigenvalue is the permittivity, not the frequency. Another important feature of the described approach is that the properties of plasmons actually depend only on the shape of the particle, not on the specific material of the resonator. Both these factors make the ‘ ε -method’ extremely useful in a wide variety of applications and problems. Moreover, one can say that the ‘ ε -method’ is a constructive definition of localized plasmons.

2.2.4 Perfect nonradiating modes. Usually, the modes of open resonators are found by solving the homogeneous Maxwell equations with the Sommerfeld radiation conditions at infinity (5) and, therefore, such modes are *fundamentally* related to radiation losses. Moreover, such modes increase unlimitedly at infinity, requiring the development of very complex artificial approaches to describe them (see, for example, [46, 52–59]).

However, finding all modes is a nontrivial task, and the quasi-normal modes studied recently in [18–23, 27–38] do not exhaust all solutions of the sourceless Maxwell equations in open nanoresonators. Quite recently in [39–41], a fundamentally new class of eigen oscillations in nanoresonators was found—perfect nonradiating modes that are solutions of sourceless Maxwell’s equations and fundamentally do not contain waves that carry energy away.

More specifically, in [40], it was proposed to search for the electromagnetic fields outside the nanoresonator in the form of a superposition of solutions of Maxwell’s equations that are nonsingular in unbounded free space. This approach is fundamentally different from the usual one assuming that the functions describing the fields outside the resonator can have singularities upon analytic continuation to the region inside the resonator. For example, in the expansion of any field component $E(r, \theta, \varphi, \omega)$ outside the resonator in terms of spherical harmonics, $Y_n^m(\theta, \varphi)$, in accordance with the Sommerfeld radiation condition, the spherical Hankel functions $h_n^{(1)}(k_0 r)$, which are *singular* at $r = 0$ (inside the resonator), are usually used:

$$E(r, \theta, \varphi, \omega) \sim \sum a_{nm} h_n^{(1)}(k_0 r) Y_n^m(\theta, \varphi). \quad (12)$$

In [40] to find the fields of nonradiating modes outside the resonator, it was proposed to use only functions that are *nonsingular* inside the resonator, for example, the spherical Bessel functions, $j_n(kr)$, so that, instead of (12), the asymptotic form of the fields has the form

$$E(r, \theta, \varphi, \omega) \sim \sum a_{nm} j_n(k_0 r) Y_n^m(\theta, \varphi). \quad (13)$$

Obviously, if the solution of (4) with the asymptote (13) exists, then in principle it will not have a flux of energy and radiation at infinity!

Since (13) has no singularities in the entire space, the initial problem of finding fields in infinite space can be reduced to that of finding fields only inside the nanoresonator. As a result, the system of equations that determines nonradiating modes in a nanoparticle with the permittivity ε can be written as a system of two equations for two auxiliary fields $\mathbf{E}_1, \mathbf{E}_2$ inside the region V , determining the resonator:

$$\begin{aligned} \nabla \times \mathbf{E}_1 &= ik_0 \mathbf{H}_1, & \nabla \times \mathbf{H}_1 &= -ik_0 \varepsilon \mathbf{E}_1, & \mathbf{r} &\in V, \\ \nabla \times \mathbf{E}_2 &= ik_0 \mathbf{H}_2, & \nabla \times \mathbf{H}_2 &= -ik_0 \mathbf{E}_2, & \mathbf{r} &\in V, \end{aligned} \quad (14)$$

connected only through the conditions for the continuity of the tangential components of the electric and magnetic fields

$$\mathbf{E}_{t,1} = \mathbf{E}_{t,2}, \quad \mathbf{H}_{t,1} = \mathbf{H}_{t,2} \quad (15)$$

on the surface of the resonator.

At some *real* values of frequency or permittivity, the system (14), (15) becomes consistent, meaning the appearance of ‘perfect’ nonradiating modes. The physical fields inside the resonator are equal to $\mathbf{E}_1, \mathbf{H}_1$, while the physical fields outside the particle are determined by the analytical continuation of the auxiliary solution $\mathbf{E}_2, \mathbf{H}_2$ into the outside region.

The modes found in this way form an orthogonal system and have no analogues. In particular, they differ from so-called anapole current distributions [19, 31–36] in that, unlike the latter, their fields outside the particle are nonzero and have well-defined expansions in spherical harmonics (13). These modes also differ from the ‘bound states in a continuum’ mode, as they do not decay exponentially. The perfect modes are closest to strange (merkwürdig) Neumann–Wigner modes [67], but, unlike the latter, the nanoresonator potential (permittivity) differs from the free space value only in a finite region of space, which fundamentally distinguishes perfect nonradiating modes from strange Neumann–Wigner

modes [67], where the potential is nonzero in the entire space. The complete absence of radiation makes it possible to call these modes perfect nonradiating modes.

System of equations (14), (15) is very complicated, and there is no rigorous mathematical theory for it in the general case. Nevertheless, in [40, 41], it was possible to find conditions for the existence of perfect nonradiative modes for arbitrary spheroids, hyperspheroids, and elliptical cylinders, describing well almost all nanoparticle shapes of interest for applications. Perfect nonradiating modes are not abstract solutions: they are of great importance for finding conditions when the scattered power becomes minimal or even zero, while the energy stored in the nanoresonator remains finite. This leads to an unlimited increase in the Q -factor of these modes (see Sections 4.1.2, 4.2.2, 4.3.3).

2.3 Anapole current distributions and eigenmodes

The concept of *anapole* was introduced by Zel'dovich [68] to designate a current with electromagnetic fields equal to zero where this current is absent. Anapole is the simplest representative of the family of Cartesian toroidal (anapole) multipoles, necessary (along with Cartesian electric and magnetic multipoles) for a complete description of the field of arbitrary current sources. An illustrative model of a toroidal anapole is a torus-shaped solenoid with the current flowing through its winding. A change in the anapole (toroidal) moment with time leads, in the general case, to the emission of electromagnetic radiation. However, there are such distributions of charge densities and currents, $\rho(\mathbf{r}), \mathbf{J}(\mathbf{r})$, when the fields of Cartesian electric multipoles

$$Q_{l,m} \sim \int Y_{lm}^* \frac{\partial}{\partial r} [rj_l(kr)] \rho(\mathbf{r}) d^3\mathbf{r} \quad (16)$$

and Cartesian toroidal multipoles

$$T_{l,m} \sim \int Y_{lm}^* j_l(kr) [\mathbf{r}\mathbf{J}(\mathbf{r})] d^3\mathbf{r} \quad (17)$$

completely cancel each other out. Sometimes, these current distributions are called anapole states or even anapole modes (see Section 4.1.3). Such definitions, of course, are not correct, since modes, by definition, are solutions of the sourceless Maxwell equations.

2.4 Symmetry properties of modes in optical nanoresonators

The spatial structure of the eigenmodes of resonators is rigidly related to the symmetry of the shape of the resonators. In [69, 70], an algorithm was developed for classifying eigenmodes in resonators of the simplest shapes depending on their symmetry group. For each mode type \mathbf{E}_n , its vector multipole content is found:

$$\mathbf{E}_n(\mathbf{r}) = \sum a_n \mathbf{M}_{nmp}(\mathbf{r}) + \sum b_n \mathbf{N}_{nmp}(\mathbf{r}), \quad (18)$$

where \mathbf{M} and \mathbf{N} are the magnetic and electric vector spherical harmonics, respectively [51]. Relation (18) creates a bridge between modal and multipole descriptions.

The authors of [69] claim that their approach can be used to design, predict, and explain the scattering phenomena and optical properties of nanoresonators based only on their symmetry without the need for numerical simulations. However, despite the useful qualitative picture of the multipole composition of modes of a certain symmetry, without

numerical analysis, it is apparently impossible to say whether the multipoles in (18) are suppressed or not for specific resonator shapes (see also Section 4.3.2).

2.5 Perturbation theory methods for describing the properties of optical nanoresonators

2.5.1 Rayleigh method (quasi-statics). As early as 1897, Rayleigh showed in [71] that, to describe the scattering of light by nanoparticles, one can often use the perturbation theory with respect to a small parameter

$$ka = \frac{\omega a}{c} = \frac{2\pi a}{\lambda} \ll 1, \quad (19)$$

where a is the characteristic size of a nanoparticle and λ is the wavelength of radiation in the surrounding space. In [72, 73], this method was further developed. As applied to nanoresonators, this approach can be formulated as follows [1]. Within the framework of this approach, all fields are searched for in the form of series in powers of k :

$$\begin{aligned} \mathbf{E} &= \mathbf{E}^{(0)} + k\mathbf{E}^{(1)} + k^2\mathbf{E}^{(2)} + \dots, \\ \mathbf{H} &= \mathbf{H}^{(0)} + k\mathbf{H}^{(1)} + k^2\mathbf{H}^{(2)} + \dots, \end{aligned} \quad (20)$$

while the permittivity $\varepsilon(\omega)$ is not expanded in powers of k (frequency).

Further, by substituting such series into Maxwell's equations and equating to zero the terms at the same powers of k , the system of Maxwell's equations can be reduced to a set of potential theory problems. In particular, the eigenvalues ε_n and the eigenfunctions \mathbf{E}_n of the 'ε method' (see Section 2.2.3) can be found in the first approximation by solving the equations

$$\nabla(\varepsilon(\mathbf{r})\mathbf{E}_n) = 0, \quad \nabla \times \mathbf{E}_n = 0; \quad (21)$$

using substitution, $\mathbf{E}_n = -\nabla\varphi_n$ can be reduced to the solution of the Laplace equations

$$\Delta\varphi_n^{\text{in}} = 0, \quad \Delta\varphi_n^{\text{out}} = 0, \quad \varepsilon_n \frac{\partial\varphi_n^{\text{in}}}{\partial\mathbf{n}} \Big|_S = \bar{\varepsilon} \frac{\partial\varphi_n^{\text{out}}}{\partial\mathbf{n}} \Big|_S. \quad (22)$$

In (22), $\bar{\varepsilon}$ is the permittivity of the space surrounding the nanoresonator, $\varphi_n^{\text{in}}, \varphi_n^{\text{out}}$ stand for the potentials of the eigenfunctions inside and outside the particle, respectively, and $\partial\varphi_n/\partial\mathbf{n}|_S$ denotes the normal derivative at the boundary of the particle. The last equation in (22) ensures that the normal components of the induction or the tangential components of the magnetic field are continuous. In this case, the solution of Maxwell's equations with given excitation fields (10) remains the same. Note that, in this case, to describe plasmon oscillations, there is no need to find magnetic fields at all.

The quasi-static description of plasmon resonances (22) in nanoparticles is much simpler than the complete system of Maxwell's equations, because, instead of the Helmholtz equations, one has to solve the Laplace and Poisson equations. The solution of the Laplace and Poisson equations can be found for nanoresonators of various shapes.

The most important feature of the quasi-static description (22) is that it allows dealing only with plasmon oscillations. Other particle modes (whispering gallery modes, etc.) do not appear in this description and do not make it difficult to obtain and interpret the results.

From a mathematical point of view, the quasi-static ‘ ε -method’ differs from the full ‘ ε -method’ in that, in the former, the resonant values of the permittivity ε_n are negative real numbers. The absence of an imaginary part in the resonant values of the permittivity ε_n is due to the fact that there is no radiation in the quasi-static approximation, while the imaginary parts of ε_n arise precisely due to radiation losses.

Based on the foregoing, we conclude that the quasi-static ‘ ε -method’ describes well exactly the plasmon part of the spectrum and can be effectively used to determine the properties of localized plasmons.

Naturally, the substitution of ε_n and mode distributions $\mathbf{E}_n = -\nabla\varphi_n$ found in the quasi-static approximation into (11) makes it possible to find fields only in the near zone. Nevertheless, the quasi-static approach allows finding not only the natural frequencies ω_n of eigen oscillations (by solving the equation $\varepsilon(\omega_n) = \varepsilon_n$) but also their Q -factors (2), where the expressions for the energy stored in the resonator and the radiated power have the form

$$W_{n,\text{stored}} = \frac{d(\omega_n \varepsilon(\omega_n))}{d\omega_n} \int_V dV |\mathbf{E}_n|^2, \quad P_{n,\text{rad}} = \frac{\omega k^3}{3} |\mathbf{d}_n|^2, \quad (23)$$

$$\mathbf{d}_n = \frac{\varepsilon(\omega_n) - 1}{4\pi} \int_V dV \mathbf{E}_n,$$

where \mathbf{d}_n is the electric dipole moment of the n th mode of the nanoresonator.

2.5.2 Perturbation theory for large permittivity. The Rayleigh–Stevenson method (see Section 2.5.1) can also be applied to dielectric resonators with a large positive permittivity, when the dimensions L are small with respect to the wavelength λ_{diel} inside the body, $L \ll \lambda_{\text{diel}} = \lambda_0/N$, where N is the refractive index of the nanoresonator, $N = \sqrt{\varepsilon} \rightarrow \infty$. This limitation obviously excludes the study of nanocavities with a high permittivity, where the resonator size is smaller than the wavelength in vacuum λ_0 but larger than the wavelength in the resonator material $\lambda_0 \gg L \geq \lambda_{\text{diel}} = \lambda_0/N$.

As the refractive index N tends to infinity, it makes sense to focus on a specific resonant mode corresponding to a *finite* wave number k in the dielectric to understand what happens with the fields as $N \rightarrow \infty$ [74]. During this passage to the limit, kL approaches an asymptotic value that is finite and nonzero. This value is a characteristic of the mode. The wave number k_0 in vacuum during such a passage ($k_0 = 2\pi/\lambda_0 = k/N = \omega/c_0$) approaches zero along with the frequency, and the wavelength λ_0 tends to infinity. In [74], it was proposed to search for the modes of such nanoresonators by expanding the fields into series:

$$\mathbf{H} = \mathbf{H}_0 + \frac{\mathbf{H}_2}{N^2} + \dots, \quad \mathbf{E} = \frac{\mathbf{E}_1}{N} + \frac{\mathbf{E}_3}{N^3} + \dots \quad (24)$$

As a result, in the zeroth approximation, the natural oscillation frequencies $\omega_m = ck_m/N$ and their spatial structure can be found from the system of equations

$$\begin{aligned} \nabla \times \nabla \times \mathbf{H}_m &= k_m^2 \mathbf{H}_m \text{ inside the resonator,} \\ \nabla \times \mathbf{H}_m &= 0 \text{ outside the resonator,} \\ \nabla \mathbf{H}_m &= 0 \text{ everywhere.} \end{aligned} \quad (25)$$

In the particular case of axisymmetric nanoresonators, there can be a subset of modes — so-called confined modes with the

magnetic fields equal to zero outside the resonator in the limit $\varepsilon \rightarrow \infty$ and satisfying the equations

$$\nabla \times \nabla \times \mathbf{H}_m = k_m^2 \mathbf{H}_m \text{ inside the resonator,} \quad (26)$$

$$\mathbf{H}_m = 0 \text{ at the resonator boundary.}$$

The electric fields have a higher order of smallness and can be found from the relation

$$\mathbf{E}_m = \frac{i}{k_m N} \nabla \times \mathbf{H}_m. \quad (27)$$

In this case, despite the tendency of the electric field to zero, the energy of the electric field in the resonator remains finite.

Van Bladel’s approach [74] is extremely important, not only because of the possibility of constructing a good perturbation theory, but also because it allows one to understand the general properties of arbitrarily shaped dielectric nanoresonators. In particular, using this approach, van Bladel [74] showed that, for resonators with a very high permittivity, the radiation quality factor Q_{rad} depends on ε as

$$Q_{\text{rad}} \sim \varepsilon^P, \quad (28)$$

where $P = 1.5$ for modes radiating as a magnetic dipole (nonconfined modes, see (25)) and $P = 2.5$ for modes radiating as an electric dipole (confined modes (26)), as well as for modes radiating like a magnetic quadrupole.

Equation (28) and the P values given above are quite general and are valid regardless of the shape of the resonator. However, they have a good accuracy only for large values of ε . For example, for confined TM modes of axisymmetric nanoresonators with $\varepsilon = 80$, from (28) we get $Q = 57,000!$

In [75], based on (28), more accurate approximation formulas were found for the quality factors of dielectric nanocylinders with different aspect ratios.

2.5.3 Generalized Brillouin–Wigner perturbation theory. In Sections 2.5.1 and 2.5.2, perturbation theories were considered based on the smallness of the resonator dimensions relative to the wavelength or on the smallness of $1/\varepsilon$ for the material of the resonator. The Wigner–Brillouin perturbation theory [30, 69, 76, 77] is based on the smallness of shape variations of resonators with a known set of eigenfunctions and eigenvalues. As a rule, spherical resonators are chosen as unperturbed resonators. For a sphere, a complete set of eigenfunctions is known — they are vector spherical harmonics with normalization (8). The expansion of any mode \mathbf{E}_n of a resonator with permittivity inhomogeneities $\Delta\varepsilon(\mathbf{r})$,

$$\nabla \times \nabla \times \mathbf{E}_n = (\varepsilon^* + \Delta\varepsilon(\mathbf{r})) \frac{\Omega_n^2}{c^2} \mathbf{E}_n, \quad (29)$$

can be represented as

$$\mathbf{E}_n(\mathbf{r}) = \sum_s C_{ns} \mathbf{Y}_s(\mathbf{r}), \quad (30)$$

where Ω_n is the complex eigenfrequency of the mode \mathbf{E}_n , $\mathbf{Y}_s(\mathbf{r})$ is the eigenfunction of a sphere with permittivity ε^* , and complex eigenfrequency ω_s , and s is the composite index that includes polarization and orbital, azimuthal, and radial quantum numbers.

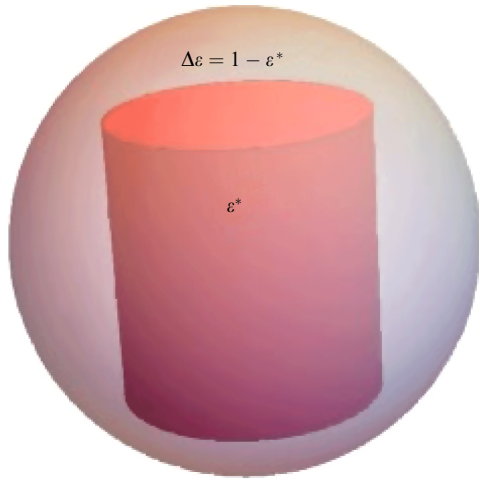


Figure 2. Illustration of the application of Brillouin–Wigner perturbation theory via the example of a cylinder inside a spherical region. A perturbation $\Delta\epsilon = 1 - \epsilon^*$ outside the cylinder is introduced into a sphere with permittivity ϵ^* . As a result, the perturbed resonator has the shape of a cylinder with permittivity ϵ^* .

From the generalized Wigner–Brillouin perturbation theory, the dispersion equation can be obtained:

$$\frac{1}{\omega_{s'}} \sum_s C_{ns} [\delta_{ss'} + V_{ss'}] = \frac{1}{\Omega_n} C_{ns'}, \quad (31)$$

where the overlap integral

$$V_{ss'} = \frac{1}{2\epsilon^*} \int dV \Delta\epsilon(\mathbf{r}) \mathbf{Y}_s \mathbf{Y}_{s'} \quad (32)$$

describes the interaction between different unperturbed modes of a spherical resonator due to its small deformation.

The inhomogeneity of the permittivity, $\Delta\epsilon(\mathbf{r})$, can be chosen so that, in fact, (29) will describe a resonator different from a spherical one. It is important that this resonator be inside the initial spherical resonator, otherwise the convergence will be poor. For example, if we choose $\Delta\epsilon = 1 - \epsilon^*$ in the region between the cylinder inscribed in the original sphere and the surface of the sphere, then (31) will describe the natural oscillations of the cylinder (Fig. 2). Applications of this method will be discussed in Section 4.

2.6 Numerical methods for describing the properties of optical nanoresonators

Usual quasi-normal modes, their eigenfrequencies, and their Q -factors are relatively easy to find by calculating spectra of light scattering by nanoparticles making use of the commercial packages Comsol [78] or CST Studio Suite [79]. In addition, these packages allow one to set a specific spatial structure of incident beams for excitation and studying modes that cannot be detected under a plane wave illumination.

The same packages can also be used conveniently to find expansion coefficients in various methods of perturbation theory. A more detailed analysis of usual modes of open resonators using the same packages can be found, for example, using the numerical approach proposed in [80, 81].

To analyze natural frequencies, one can also use the numerical solution of surface or volume integral equations. These methods are highly efficient, because they have smaller dimensions. However, these algorithms are complex and must be implemented manually (see, for example, [61]).

3. Modes in plasmonic nanoresonators

The uniqueness of plasmonic nanoresonators lies in the fact that metal nanoparticles have natural oscillation frequencies in the optical range, from the ultraviolet (UV) to infrared (IR) ranges. On the other hand, there are many methods for creating plasmonic nanoparticles, including colloid chemistry and electron nanolithography. Finally, the properties of plasmonic nanoresonators can be understood in the first approximation using the quasi-static approximation (see Section 2.5.1). All this led to the rapid development of research on the resonance properties of plasmonic nanoparticles [1].

3.1 Optical properties of spherical plasmonic resonators

The spherical geometry is unique and allows one to describe in detail all optical properties of spherical nanoresonators, which are completely determined by the poles of the reflection coefficients of spherical waves of different polarization incident upon a spherical particle of an arbitrary size and composition [1, 51, 82]:

$$q_n = \frac{\epsilon_1 \frac{d}{dz_2} [z_2 j_n(z_2)] j_n(z_1) - \epsilon_2 \frac{d}{dz_1} [z_1 j_n(z_1)] j_n(z_2)}{\epsilon_1 \frac{d}{dz_2} [z_2 h_n^{(1)}(z_2)] j_n(z_1) - \epsilon_2 \frac{d}{dz_1} [z_1 j_n(z_1)] h_n^{(1)}(z_2)}, \quad \text{TM polarization,} \quad (33)$$

$$p_n = \frac{\mu_1 \frac{d}{dz_2} [z_2 j_n(z_2)] j_n(z_1) - \mu_2 \frac{d}{dz_1} [z_1 j_n(z_1)] j_n(z_2)}{\mu_1 \frac{d}{dz_2} [z_2 h_n^{(1)}(z_2)] j_n(z_1) - \mu_2 \frac{d}{dz_1} [z_1 j_n(z_1)] h_n^{(1)}(z_2)}, \quad \text{TE polarization.} \quad (34)$$

Here, $z_{1,2} = \sqrt{\epsilon_{1,2} \mu_{1,2}} k_0 a = k_{1,2} a$, a is the resonator radius, and $\epsilon_{1,2}$, $\mu_{1,2}$ stand for permittivity and permeability of the sphere (index 1) and the surrounding space (index 2), respectively.

For plasmonic nonmagnetic nanoresonators in vacuum, the dispersion equations for the frequencies of dipole, quadrupole, and octupole resonances can be found from (33) by expanding denominators over the small size parameter $k_0 a$ [1]:

$$\begin{aligned} \epsilon_{\text{res},1}(\omega) + 2 + \frac{12}{5} (k_0 a)^2 + 2i(k_0 a)^3 + \dots &= 0, \\ \epsilon_{\text{res},2}(\omega) + \frac{3}{2} + \frac{5}{14} (k_0 a)^2 + \frac{65}{392} (k_0 a)^4 + \frac{i}{12} (k_0 a)^5 + \dots &= 0, \\ \epsilon_{\text{res},3}(\omega) + \frac{4}{3} + \frac{56}{405} (k_0 a)^2 + \frac{11788}{601425} (k_0 a)^4 \\ + \frac{469672}{95954625} (k_0 a)^6 + \frac{4i}{2025} (k_0 a)^7 + \dots &= 0, \end{aligned} \quad (35)$$

where, as usual $k_0 = \omega/c$. It is important to note that the imaginary parts of the resonant permittivity (which are associated with radiation losses) appear in higher and higher orders in powers of $k_0 a$ with increasing multipole order. This is due to the smallness of the corresponding radiation intensities and leads to huge values of the Q -factors of such natural oscillations.

Plasmon oscillations under conditions (35) take place for arbitrarily small spheres and are of great importance in various applications.

Potentials of quasi-static electric fields corresponding to resonances (35) can be found from (22) and have a simple form:

$$\Phi_n^m = \begin{cases} \left(\frac{r}{a}\right)^n Y_n^m(\theta, \varphi), & r < a, \\ \left(\frac{a}{r}\right)^{n+1} Y_n^m(\theta, \varphi), & r > a. \end{cases} \quad (36)$$

It is very similar to the solution to the quantum mechanical problem for the hydrogen atom.

Expressions (35), (36), together with the solution to the general scattering problem within the framework of the ‘ ε -method’ (11), give a good description of all optical properties of spherical plasmonic nanoresonators.

Despite the fact that the electric fields of natural oscillations in plasmonic nanoresonators are described by simple spherical harmonics, the energy flows have a rather complicated form, even for very small nanoresonators. In particular, it was shown in [83–85] that near the resonances there are nontrivial vortices in the pattern of energy flows inside and around the resonator. When weak dissipation is taken into account, these vortices terminate inside the sphere [86].

A very interesting regime of scattering of a converging spherical wave $h_n^{(2)}(k_0 r)$ by a plasmonic sphere was found in [87], where it was shown that, if the condition

$$\varepsilon_1 \frac{d}{dz_2} [z_2 h_n^{(2)}(z_2)] j_n(z_1) = \varepsilon_2 \frac{d}{dz_1} [z_1 j_n(z_1)] h_n^{(2)}(z_2) \quad (37)$$

is fulfilled, the reflected spherical wave proportional to $h_n^{(1)}(k_0 r)$ is completely absent and the solution of Maxwell’s equations turns into a single vortex, starting at infinity and ending at the center of the sphere, that is, coherent perfect absorption appears. Note that condition (37) coincides with the condition of vanishing of the complex conjugate denominator of the Mie coefficient (33), and therefore the solution found in [87] can be considered a time-reversed solution for a spaser [2].

A converging spherical wave $h_n^{(2)}(k_0 r)$, resulting in perfect absorption, cannot be accurately realized in practice. Therefore, to realize perfect coherent absorption by a plasmonic nanoparticle, a specially selected superposition of radially polarized Bessel beams in the form

$$E_{\text{in}}(\mathbf{r}) = \begin{pmatrix} E_\rho \\ E_\varphi \\ E_z \end{pmatrix} = \int_0^{k_0} dk_\rho E_0(k_\rho) \begin{pmatrix} ik_z J_1(k_\rho \rho) \\ 0 \\ k_\rho J_0(k_\rho \rho) \end{pmatrix} \times \exp\left(-i\sqrt{k_0^2 - k_\rho^2} z\right) \quad (38)$$

was used in [88]. In (38), the weight function $E_0(k_\rho)$ should be chosen to achieve complete absorption. Assuming that the absorbing nanoparticle can be described in the dipole approximation, an explicit form for $E_0(k_\rho)$ was found in [88].

3.2 Optical properties of spheroidal and ellipsoidal plasmonic resonators

The optical properties of spheroidal and ellipsoidal plasmonic resonators can also be found in the framework of the quasi-static approximation.

For prolate spheroids with semi-axes $a = b < c$, the dispersion equation that determines the frequencies of

plasmon oscillations has the form [1]

$$\varepsilon(\omega_n^m) = \varepsilon_n^m = \frac{(Q_n^m(\xi_0))' P_n^m(\xi_0)}{(P_n^m(\xi_0))' Q_n^m(\xi_0)}, \quad (39)$$

where the parameter $\xi_0 = c/\sqrt{c^2 - a^2}$, and P_n^m , Q_n^m are the associated Legendre polynomials of the first and second kind, respectively. Corresponding to (39), the distributions of mode potentials have the form

$$\varphi_n^m = P_n^m(\eta) P_n^m(\xi) Q_n^m(\xi_0) \begin{bmatrix} \cos(m\varphi) \\ \sin(m\varphi) \end{bmatrix}, \quad \xi < \xi_0, \quad (40)$$

$$\varphi_n^m = P_n^m(\eta) P_n^m(\xi_0) Q_n^m(\xi) \begin{bmatrix} \cos(m\varphi) \\ \sin(m\varphi) \end{bmatrix}, \quad \xi > \xi_0,$$

where η , ξ , and φ are prolate spheroidal coordinates [89]. For a plasmonic nanoresonator in the form of an oblate spheroid, these expressions are also valid after the corresponding analytical continuation.

The most common form of a plasmonic nanoresonator with known natural frequencies is a triaxial nanoellipsoid [1, 90, 91]. For an arbitrary plasmonic resonator in the form of a nanoellipsoid with semi-axes $a_1 > a_2 > a_3$ along each axis of the Cartesian coordinate system x_1, x_2, x_3 , the dispersion equation that determines the frequencies of plasmon oscillations ω_n^m has the form

$$\varepsilon(\omega_n^m) = \varepsilon_n^m(a_1, a_2, a_3) = \frac{E_n^m(a_1; a_1, a_2, a_3) F_n^m(a_1; a_1, a_2, a_3)}{E_n^m(a_1; a_1, a_2, a_3) F_n^m(a_1; a_1, a_2, a_3)}. \quad (41)$$

For the eigenfunctions of plasmon oscillations, respectively, we have the expressions

$$\varphi_n^m = E_n^m(\mu; a_1, a_2, a_3) E_n^m(\nu; a_1, a_2, a_3) \times \begin{cases} F_n^m(a_1; a_1, a_2, a_3) E_n^m(\rho; a_1, a_2, a_3), & \rho \leq a_1, \\ E_n^m(a_1; a_1, a_2, a_3) F_n^m(\rho; a_1, a_2, a_3), & \rho > a_1. \end{cases} \quad (42)$$

In (41), (42), F_n^m , E_n^m are the external and internal Lamé functions, respectively, and ρ , μ , and ν are ellipsoidal coordinates [92], the values of n are natural numbers, and m varies from 1 to $2n + 1$, as in spherical harmonics. Figure 3 [90] shows the dependences of the eigenfrequencies of the lowest plasmon oscillations on the aspect ratio a_3/a_1 in a nanoellipsoid with the permittivity described by the Drude law:

$$\varepsilon(\omega) = 1 - \frac{\omega_{\text{pl}}^2}{\omega^2}. \quad (43)$$

In [90], plots of eigenfrequencies for higher-order modes are also presented.

In a triaxial ellipsoid, there is no axial symmetry, and therefore the eigenvalues degenerated in the case of a sphere split into $2n + 1$ different ones. Moreover, as the parameters of the ellipsoid change, these eigenvalues change in a nonmonotonic and nontrivial way. This is extremely important, since it enables effective control of optical processes where there are several frequencies, for example, to create bright artificial fluorophores [91].

Equations (41), (42) exhaust the solution to the problem of plasmon oscillations in a triaxial nano-ellipsoid in the quasi-static (Rayleigh) approximation. Corrections due to retardation effects and explicit expressions for the eigenfunc-

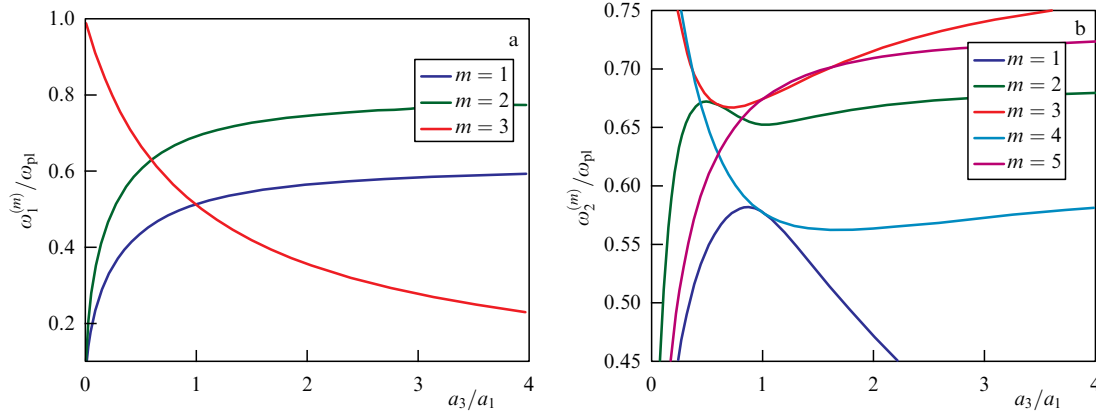


Figure 3. Eigenfrequencies of plasmonic oscillations of a triaxial ellipsoid as a function of the ratio of semiaxes a_3/a_1 (for $a_2/a_1 = 0.6$). Solutions are shown in the following cases: (a) $n = 1$; (b) $n = 2$ [90].

tions of ellipsoidal resonators in Cartesian coordinates can be found in [90].

The effect of the mode structure in a silver nanospheroid on the temporal dynamics of plasmon oscillations in it was considered in [93], where it was shown that the use of only two quasi-normal modes to describe such a nanoparticle explains well the experimental data on measuring ultrafast dynamics using photoemission electron microscopy (PEEM) [94].

3.3 Optical properties of clusters of plasmonic resonators

In Sections 3.1 and 3.2, we have presented the results of studies on plasmonic resonances in isolated particles that are topologically equivalent to a sphere. Even more interesting resonant oscillations are possible in nanoparticle clusters, since they have a more complex geometry and a larger number of control parameters.

In [95–97], an analytical description of the resonant properties of oscillations in a dimer of two spherical nanoparticles was developed.

Figure 4 shows the dependences of eigenfrequencies of transverse oscillations ($m = 1$) of a plasmonic dimer on the distance between nanoparticles. The L - and T -modes are

associated with the hybridization of the modes of individual nanoparticles [98, 99], while the high-frequency M -modes, which appear only at short distances $R_{12}/(2R_0) \leq 1.2$, have no equivalent and correspond to bound states that arise in the strong interaction regime.

For the eigenfrequencies of the M -modes, the analytical solution has the form [95–97]

$$\omega_m^{(M)} = \frac{\omega_{pl}}{\sqrt{1 - \epsilon_m^{(M)}}},$$

$$\epsilon_m^{(M)} = -(m + M + \delta_m) \operatorname{arsinh} \sqrt{\frac{R_{12}^2}{4R_0^2} - 1}, \quad (44)$$

$$m = 0, 1, 2, \dots, \quad M = 1, 2, 3, \dots$$

The corrections δ_m are independent of the mode number M and are equal to $[1/2, -0.08578, -0.2639, -0.33, -0.3769, -0.4, -0.4172, 0.4289, -0.4377, -0.4446]$ for $m = 0-9$, respectively. These expressions show that, as the nanoparticles approach each other, the resonant frequencies of the M -modes of the dimer tend to the plasma frequency ω_{pl} .

For L -modes, there is a similar analytical solution [95–97]:

$$\omega_m^{(L)} = \frac{\omega_{pl}}{\sqrt{1 - \epsilon_m^{(L)}}},$$

$$\epsilon_m^{(L)} = -\frac{(m + L - 1/2)^{-1}}{\operatorname{arsinh} \sqrt{R_{12}^2/(4R_0^2) - 1}} + \dots, \quad (45)$$

$$m = 0, 1, 2, \dots, \quad L = 1, 2, \dots,$$

that is, as the nanospheres approach each other, the resonant frequencies of the L -modes of the dimer tend to zero.

Figure 5 shows the spatial distribution of the potential of the longitudinal M -, L -, T -modes ($m = 0$). It can be seen from Fig. 5 that the spatial structure of antisymmetric (L -modes) and symmetric (T -modes) wave functions generally corresponds to that of wave functions of isolated plasmonic nanoresonators. Namely, a positive charge is located on one hemisphere, while a negative charge equal to it due to the electroneutrality of the sphere is located on the opposite side of the sphere. In this case, the interaction between plasmonic nanoresonators is reduced to some quantitative redistribution of the charge on opposite hemispheres only.

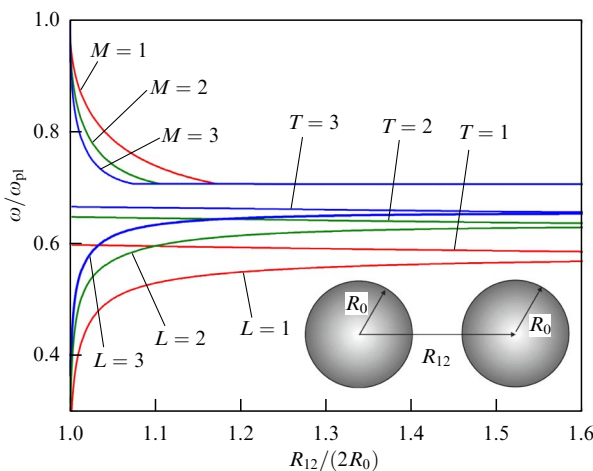


Figure 4. Eigenfrequencies of transverse plasmon oscillations ($m = 1$) in a cluster of two nanospheres depending on the distance between them. Upper part of the figure shows clearly the emergence of new modes (M -modes) at small distances between the spheres. It is assumed that the permittivity is described by the Drude law (43).

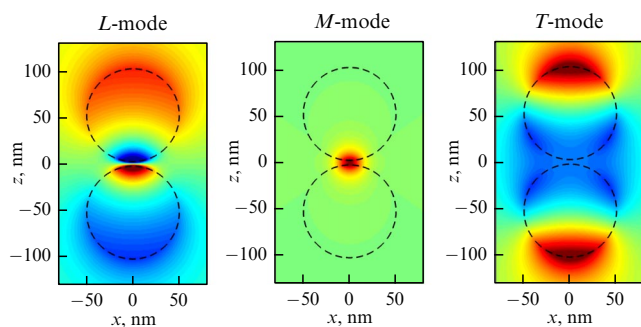


Figure 5. Spatial distribution of the potential in some plasmon modes in a cluster of two nanospheres ($m = 0$, axisymmetric longitudinal oscillations) [97].

In the case of symmetric M -modes, the situation is different, and both positive and negative charges are concentrated near the gap between the nanospheres. Actually, at points far from the gap of the nanospheres, the wave functions of M -modes vanish.

As the distance between the spheres increases, the localization of the M -modes decreases and, at a critical distance between the spheres, these modes disappear, while the hybridized L - and T -modes do not undergo significant changes.

The difference between the localizations of the M -modes and L -, T -modes determines their fundamental difference with respect to the excitation fields. L -, T -modes have a polarizability of the order of the volume of a nanosphere, $\alpha \sim R_0^3$, and effectively interact with uniform external fields of the appropriate orientation and symmetry. By contrast, M -modes have a relatively low polarizability $\alpha \sim \Delta^3$, where Δ is the gap width between the spheres. Because of this, the M -modes are weakly (compared to the L - and T -modes) excited by uniform optical fields. On the other hand, M -modes interact effectively with strongly inhomogeneous fields that are localized near the gap between the spheres. Fields of this kind arise during the radiation of atoms and molecules located near the gap. This circumstance makes the M -modes extremely promising from the point of view of creating nanosensors and elements of nanodevices that are sensitive to the radiation of individual molecules.

A similar study of the resonance properties of a cluster of two plasmonic nanospheroids was carried out in [100].

Currently, plasmonic resonant nanostructures based on DNA origami technology are being actively studied [101–109]. This technology is very promising, as it allows one to arrange nanoparticles in a nanostructure with an accuracy higher than that of modern optical or electronic nanolithography. The creation of complex three-dimensional nanostructures from nanoparticles using DNA tethers is possible based on the canonical pairing of DNA bases à la Watson–Crick [101]. This approach opens unprecedented possibilities for the control of three-dimensional macromolecular structures on large scales. Using this technology, nanostructures of nanoparticles in the form of arrays [102, 103], spirals [104], tetrahedra [105], chains [106, 107], or nanorings [108] have already been realized. Recently, the possibility of transmitting information with low losses through a plasmonic waveguide made using DNA origami technology has been demonstrated [109].

In [110], the dependence of the resonant optical properties of Platonic clusters that can be synthesized using DNA

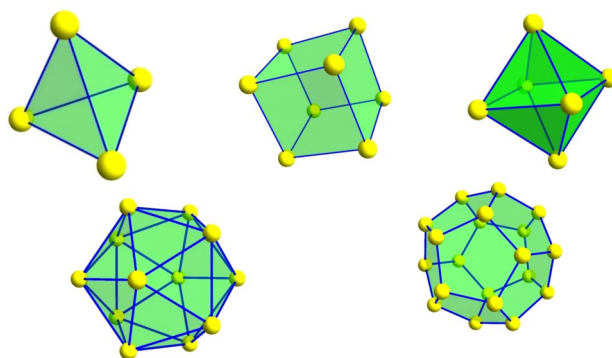


Figure 6. Platonic clusters of nanoparticles, shown as yellow balls.

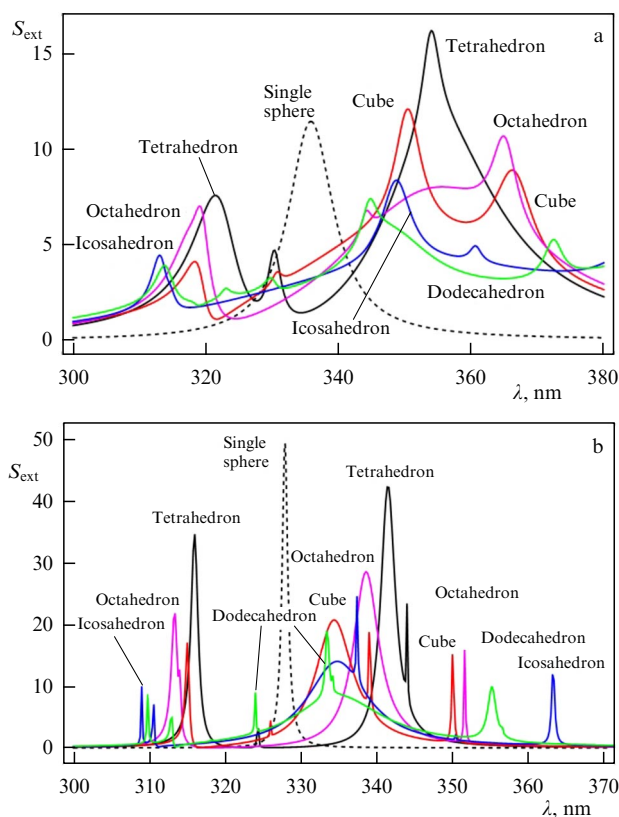


Figure 7. Comparison of extinction spectra of Platonic clusters: (a) Ag, $L_0 = 50$ nm and $R_0 = 20$ nm and (b) $L_0 = 25$ nm and $R_0 = 10$ nm (losses in the metal are reduced by a factor of 20 compared to real Ag) [110].

origami technology on their topology and size was studied (Fig. 6). To describe the optical properties of such clusters, a model was used in [110] where individual nanoparticles are characterized by isotropic polarizabilities and induced dipole moments with the interaction described by the retarded Green's function. Figure 7 shows the extinction spectra of various Platonic clusters with the same edge length L_0 and the same radius R_0 of silver particles, but with different topologies.

Comparing Fig. 7a and Fig. 7b shows that the number of observed modes of Platonic clusters effectively increases as radiation and Joule losses decrease. Therefore, Fig. 7 can serve as a guideline for understanding the optical properties of meta-atoms in the form of Platonic clusters and interpreting experimental data.

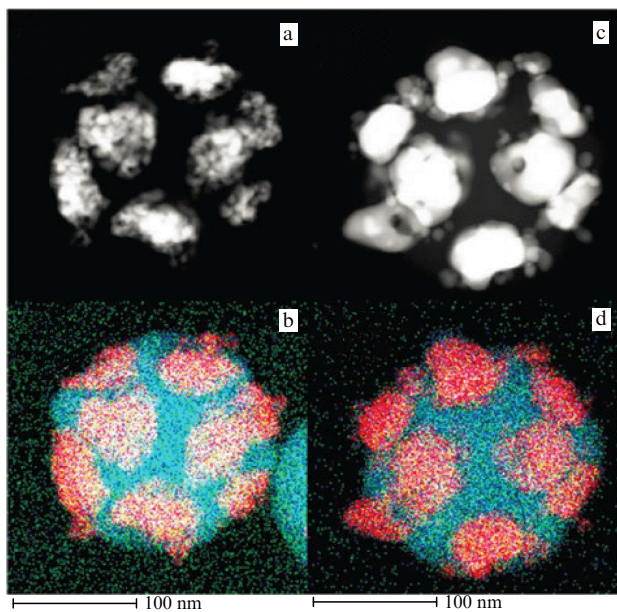


Figure 8. Synthesized dodecapods. SEM image of the dodecapods before (a) and after (c) condensation of seed nuclei. (b) and (d) show the elemental composition of the synthesized dodecapod: green color—SiO₂, red color—Au [111].

In [111], a plasmonic nanoresonator was synthesized in the form of a dodecapod consisting of a quartz core and 20 gold satellites — ‘pods’ (Fig. 8)— and it was experimentally shown that the value of the magnetic dipole moment induced in it is about 14% of the induced electric dipole moment, that is, optical magnetism has been demonstrated.

4. Modes in dielectric nanoresonators

The main advantage of the plasmonic nanoresonators considered in Section 3 is that natural oscillations can exist at arbitrarily small sizes of nanoresonators. However, the value of this fact is significantly reduced by the circumstance that the Joule losses in plasmonic resonators are quite large and, in fact, the quality factors of plasmonic nanoresonators are limited to values of the order of 10–100.

Recently, research has begun on an alternative approach to controlling light on the nanoscale. It is based on dielectric nanoresonators, that is, nanostructures made of dielectric materials with a high or moderate refractive index, such as Si, Ge, GaAs, TiO₂, and Cu₂O, and very small internal (Joule) losses. Although most dielectric nanoresonators are larger than 100 nm in one or several dimensions, they are referred to in most publications as nanospheres, nanorods, nanodisks, and so on according to their shape. We will also call them nanoresonators, since their dimensions are much smaller than the wavelength in free space.

The history of dielectric resonators began with study [47] in 1939, which laid the foundations for the theory of such resonators. An important development in this area was due to van Bladel [74], who developed the theory of resonators with a large permittivity and noted the importance of the axial symmetry of such resonators for obtaining a high quality oscillation. Dielectric resonators were developed further in microwave technology [75, 112, 113]. At present, in connection with the development of nanotechnologies, the elabora-

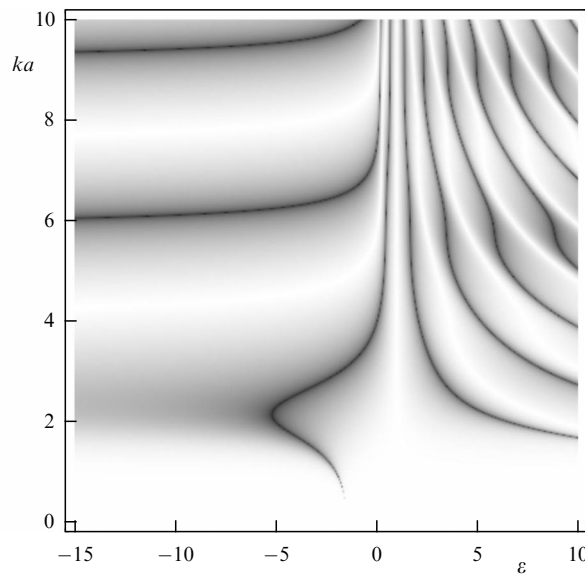


Figure 9. Dependence of the absolute value of Mie coefficients $|q_4|$ (33) on the permittivity and size parameter ka of a nonmagnetic sphere located in vacuum. Black color corresponds to a Mie coefficient equal to 1, i.e., resonance, while white color corresponds to a Mie coefficient equal to 0 (no scattering) [1].

tion of dielectric resonators in the optical range has also become possible [7, 16, 114, 115].

4.1 Spherical dielectric nanoresonators

4.1.1 Usual (quasi-normal) modes. As in the case of spherical plasmonic resonators, modes of spherical dielectric resonators are completely described by the Mie theory, that is, the scattering coefficients (33), (34). In Fig. 9, the dependence of the absolute value of the Mie coefficients q_4 (33) on the permittivity and size of the sphere is shown. It can be seen from this figure that, for subwavelength spheres, the resonance is possible only at high permittivities, when the wavelength in the dielectric becomes much smaller than the nanoresonator dimensions.

The poles of the Mie scattering coefficients at positive permittivity completely determine the eigenfrequencies of the quasi-normal modes of dielectric spheres. In the case of large permittivity $\epsilon \rightarrow \infty$, the resonant properties of the dielectric sphere were studied in detail in [74, 116, 117]. In the case of TM modes, the approach in [117] leads to the following asymptotic expressions for the eigenfrequencies and Q -factors of the three lowest modes:

$$\begin{aligned}
 k_n^{\text{TM}} a &= \frac{X_n^{\text{TM}}}{\sqrt{\epsilon}} \left(1 - \frac{1}{n\epsilon} + \dots \right), \quad Q_1^{\text{TM}} = \frac{\epsilon^{5/2}}{2(X_1^{\text{TM}})^3}, \\
 Q_2^{\text{TM}} &= \frac{18\epsilon^{7/2}}{(X_2^{\text{TM}})^5}, \quad Q_3^{\text{TM}} = \frac{2025\epsilon^{9/2}}{2(X_3^{\text{TM}})^7}, \\
 J_{n+1/2}(X_n^{\text{TM}}) &= 0.
 \end{aligned} \tag{46}$$

For TE modes, the approach in [117] leads to the expressions

$$\begin{aligned}
 k_n^{\text{TE}} a &= \frac{X_n^{\text{TE}}}{\sqrt{\epsilon}} \left(1 - \frac{1}{(2n+1)\epsilon} + \dots \right), \\
 Q_n^{\text{TE}} &= \frac{\Gamma^2(n+1/2)(4\epsilon)^{n+1/2}}{4\pi(X_n^{\text{TE}})^{2n-1}}, \quad J_{n-1/2}(X_n^{\text{TE}}) = 0.
 \end{aligned} \tag{47}$$

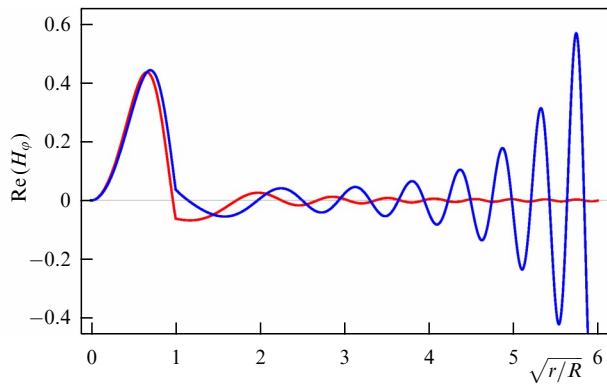


Figure 10. Dependence of $\text{Re}(H_\phi(r, \theta = \pi/2))$ on the radius for a usual quasi-normal TM_{101} mode (blue curve, $k_0 R = 1.35715 - 0.160978i$) and for a perfect nonradiating PTM_{101} mode (red curve, $k_0 R = 1.51893$) in a sphere of radius R with $\varepsilon = 10$ [40].

Comparing the Q -factors of TM and TE modes, one can see that the Q -factors of TM modes are much higher. This is due to the fact that, as shown in [74], in resonators with a large permittivity, TM modes are confined, that is, in the limit $\varepsilon \rightarrow \infty$, the magnetic field is strictly confined inside the resonator, and the electric field is zero everywhere. TE modes, by contrast, are not confined, and even in the limit $\varepsilon \rightarrow \infty$ the magnetic field of TE modes is nonzero outside the sphere. This circumstance leads to nonconfined TE modes radiating more effectively, and therefore having lower quality factors. This circumstance is general.

4.1.2 Perfect nonradiating modes. For a spherical nonmagnetic nanoresonator of radius R in vacuum, the expression for the magnetic field of the perfect nonradiating TM modes has the form [40]

$$\begin{aligned} H_\phi^{(n)} &= j_n(z_0) j_n(k_0 \sqrt{\varepsilon} r) P_n^1(\cos \theta), \quad r < R, \\ H_\phi^{(n)} &= j_n(z_1) j_n(k_0 r) P_n^1(\cos \theta), \quad r > R, \\ z_0 &= k_0 R, \quad z_1 = k_0 \sqrt{\varepsilon} R, \end{aligned} \quad (48)$$

which follows from the direct solution of Maxwell's equation.

Note that, in the case of a sphere, the condition for the existence of perfect nonradiating modes (48)

$$\varepsilon j_n(z_1) [z_0 j_n(z_0)]' = j_n^{(1)}(z_0) [z_1 j_n(z_1)]' \quad (49)$$

coincides with the vanishing of the numerator of the Mie scattering coefficient. Dispersion equation (49), along with complex roots, also has real roots, which correspond to perfect nonradiating modes. Figure 10 shows the dependences of $\text{Re}(H_\phi(r, \theta = \pi/2))$ on the radius for the perfect nonradiative PTM_{101} mode and the usual quasi-normal TM_{101} mode with radiative loss in a sphere with $\varepsilon = 10$. From Fig. 10, it can be seen that the field of the usual (quasi-normal) mode increases exponentially at infinity, while the field of the perfect nonradiating mode decreases and has no radiation losses! It was also shown in [40] that Joule losses in a dielectric have practically no effect on the properties of perfect nonradiating modes.

4.1.3 Anapole current distributions. In [32–36], the case of vanishing individual Mie scattering coefficients was studied,

but here the main attention was on demonstrating how the expansion over Cartesian multipoles when taking into account toroidal moments is consistent with the expansion over vector spherical harmonics, thus leading to a zero field outside the spheres and, accordingly, to zero radiation. In these studies, the distribution of fields inside the sphere, which leads to the compensation of the Cartesian electric dipole moment by the Cartesian toroidal electric moment, is highly incorrectly called the anapole mode, since the modes, by definition, are solutions of the Maxwell's equation in the absence of currents. From our point of view, it is more correct to talk about anapole current distributions.

4.1.4 Excitation of modes of spherical nanoresonators. To understand the practical importance of usual quasi-normal and perfect nonradiating modes, one must also consider how they can manifest themselves in practical conditions, that is, find the conditions for their excitation. There are two lines of research here. The first deals with conditions for excitation of several resonant modes simultaneously and the resulting interference phenomena in the far zone. For example, in [118], it was first noticed that, at $2\pi\sqrt{\varepsilon}R/\lambda_0 > 2.7$, the radiation pattern of light scattered by a dielectric sphere of radius R transforms from Rayleigh nondirectional scattering into forward scattering. In this paper, this effect was explained by the interference of electric and magnetic dipole moments induced in the sphere.

In [9–11], the results of [118] were generalized to the case of excitation of silicon spherical nanoresonators by radiation from a dipole source. It was shown that both electric and magnetic dipole moments can be simultaneously excited in an Si nanoresonator, and the interference of their fields can lead to directional radiation due to the complete suppression of backward scattering (Huygens element), even from a single nanoparticle [9, 11, 119]. In Si nanoparticle with a radius of 65 nm, this effect is achieved, since, in a certain frequency range ($\lambda = 570$ nm), it is possible to ensure that the electric and magnetic dipole moments induced in the particle are the same in amplitude and phase. In this case, the radiation of the dipole + nanosphere system will be directed from the dipole to the side where the nanoparticle is located. At $\lambda = 490$ nm, the electric and magnetic dipole moments induced in the same particle will have the same amplitudes, but the phases will be shifted by 1.3 radians, leading to a change in the direction of radiation in the system under consideration to the opposite one. The importance of the contribution of induced magnetic dipoles to light scattering even led to the appearance of the term 'magnetic light' [120].

Another line of research on the manifestation of optical resonances in nanoparticles is, by contrast, the detection of only one resonant mode, a quasi-normal or perfect nonradiating one. This is a more difficult task, since specially prepared light beams are needed for this, because the sphere excitation by a standard plane wave always conceals subtle effects associated with individual modes by strong fields from the excitation of a continuum of quasi-normal modes.

In [39], an exact analytical solution was found for the problem of excitation of a dielectric sphere by an axisymmetric Bessel beam:

$$\begin{aligned} H_\phi &= H_0 J_1(k_0 \rho \sin \beta) \exp(ik_0 z \cos \beta) \quad (\text{TM polarization}), \\ E_\varphi &= E_0 J_1(k_0 \rho \sin \beta) \exp(ik_0 z \cos \beta) \quad (\text{TE polarization}), \end{aligned} \quad (50)$$

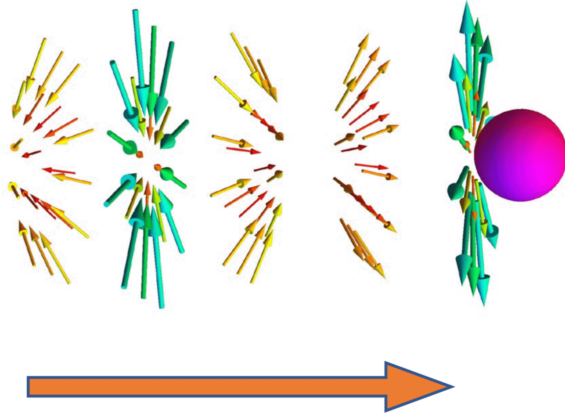


Figure 11. Structure of the electric field in an axisymmetric TM Bessel beam.

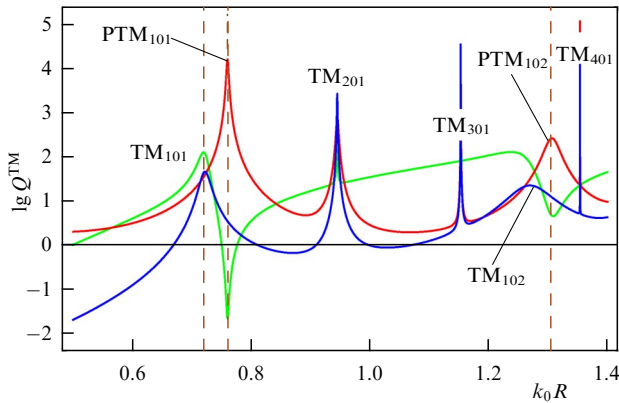


Figure 12. Dependence of generalized quality factor Q (red curve, see (3)), scattered power (green curve), and stored energy (blue curve) on the size parameter of the nanosphere k_0R (axisymmetric Bessel beam, TM polarization, $\varepsilon = 36$, $\beta = \pi/4$) [39].

where ρ and z are cylindrical coordinates, and β is the conical angle of the beam. Such a beam has a complex spatial structure (Fig. 11), enabling one to control its interaction with axisymmetric particles effectively.

The expression for the magnetic field scattered by the sphere in spherical coordinates (r, θ, φ) has the form [39]

$$H_\varphi^R(r, \theta) = iH_0 \sum_{n=1}^{\infty} i^n q_n \frac{2n+1}{n(n+1)} h_n^{(1)}(k_0r) P_n^1(\theta) P_n^1(\beta), \quad (51)$$

where q_n are the Mie coefficients (33).

Solution (51) describes the excitation of a sphere (exactly) and other axisymmetric nanoparticles (qualitatively) by axisymmetric beams having only TM or TE polarization. This solution removes the limitation imposed by the Mie 1908 solution, where the TM and TE modes cannot be separated. An important feature of solution (51) is also that it nontrivially depends on the cone angle β , whose tuning can control the excitation or suppression of certain modes.

In Fig. 12, one can see the dependence of the generalized Q -factor (3), scattered power, and stored energy on the size parameter k_0R of the nanosphere for a beam with TM polarization. Figure 12 clearly shows ultra-high quality ($Q > 10^4$) perfect modes (PTM₁₀₁) with very low scattered

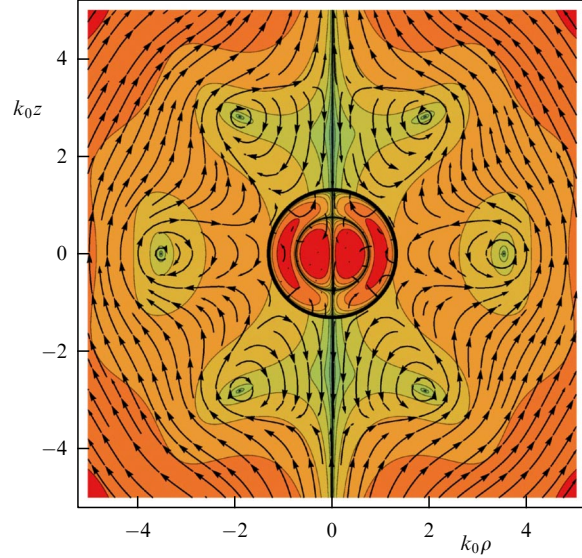


Figure 13. Practically nonradiating 32-field distribution of a magnetic field when a sphere is excited by a superposition of 4 Bessel beams ($k_0R = 1.31$, $\varepsilon = 36$) [39].

power, with the Q -factor limited only by the presence of a continuum of usual quasi-normal modes. The positions of the perfect modes correspond exactly to the solutions of dispersion equation (49).

The dependence of the solution found on the parameters of the Bessel beam makes it possible to find the conditions for the excitation of any preassigned usual or perfect mode with an unlimited radiation Q -factor.

Figure 13 shows the distribution of the magnetic field when the sphere is illuminated with a superposition of 4 Bessel beams with specially selected parameters, suppressing the lowest order mode radiation completely. As a result, only extremely weak 32-field (triacontadipole) radiation survives. Note that inside the sphere the field distribution corresponds to the pure PTM₁₀₂ mode.

Recently, in [15], an attempt was made to study experimentally TM and TE resonances in Si nanospheres separately using radially and azimuthally polarized beams. Figure 14 shows the results of such an experiment and the corresponding computer simulation. From Fig. 14, it can be seen that, for a radially polarized beam, mainly electric modes (both ED and EQ) are excited, while during excitation by an azimuthally polarized beam, mainly magnetic modes (both MD and MQ) are excited. Note that for the radial excitation there is a scattering minimum near $\lambda = 450$ nm, which probably corresponds to the perfect nonradiative mode.

4.2 Spheroidal nanoresonators

4.2.1 Quasi-normal modes. In principle, usual quasi-normal modes of spheroidal nanoresonators can be found on the basis of an analytical solution to the problem of plane wave scattering by a dielectric spheroid [121, 122]. However, we failed to find such a solution in the literature.

The case of small deviations from the spherical shape was considered in [123], where small deviations from the spherical shape were described by the expression

$$\frac{r}{R} = 1 + \mu F(\theta, \varphi) \quad (52)$$

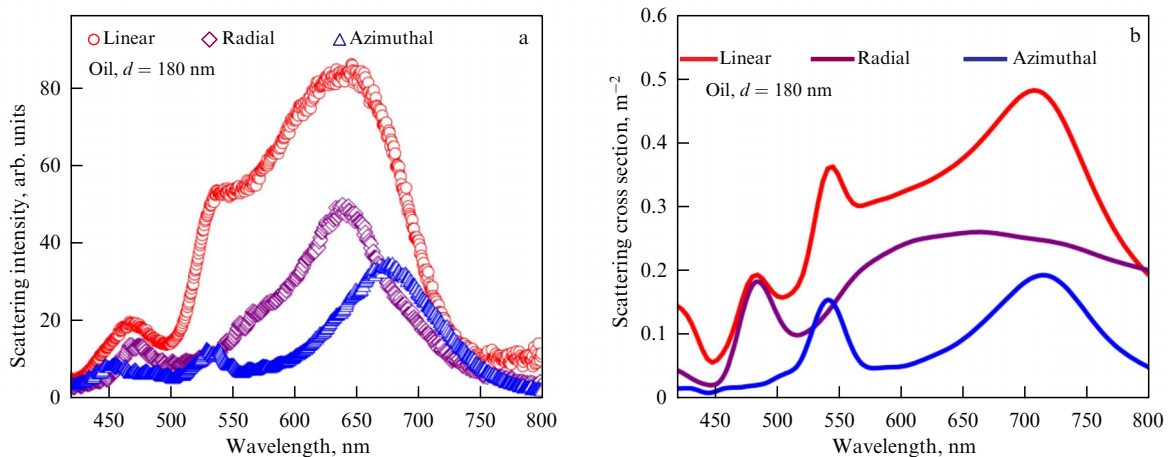


Figure 14. Selective excitation of multipole resonances using radially and azimuthally polarized beams. Experimental (a) and theoretical (b) spectra of single Si nanospheres with a diameter of 180 nm in immersion oil with $n = 1.48$ [15].

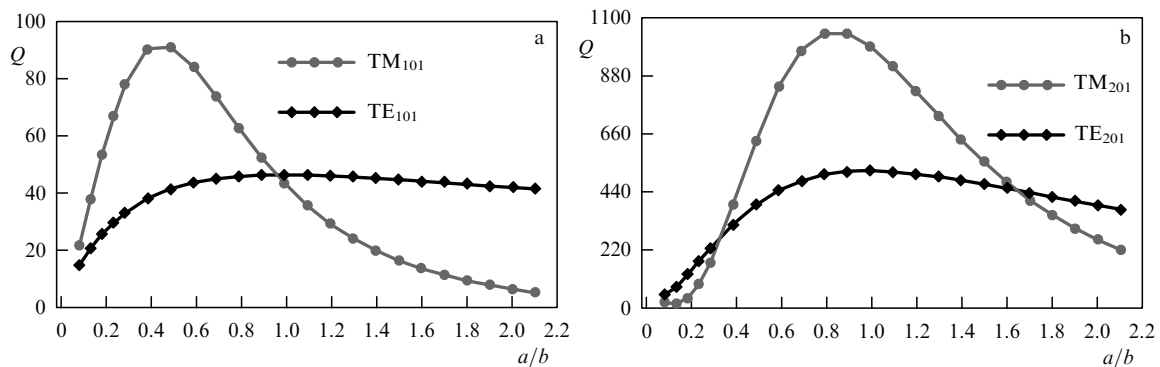


Figure 15. Dependences of the quality factors of the lowest modes for spheroids with $\varepsilon = 38$ on the aspect ratio of the semi-axes [61].

with the small parameter μ , and the change in the quality factor of the mode associated with this perturbation was sought in the form of a series

$$\frac{1}{Q} = \frac{1}{Q_0} + \mu C_1 + \mu^2 C_2 + \dots, \quad (53)$$

where $Q_0 \gg 1$ is the quality factor of the unperturbed sphere mode.

The main and most important result of [123] is that it shows that, for any high-quality mode of the sphere ($Q_0 \rightarrow \infty$) $C_1 = O(1/Q_0) \rightarrow 0$, $C_2 \geq 0$, i.e., any small shape perturbation of the high-quality spherical resonator leads to a decrease in the quality factor of its modes. This result is quite consistent with the intuitive idea of a sphere as a perfect object that minimizes the scattering of waves on its surface. In the case of not very high Q -factors, the coefficient C_1 becomes nonzero, and the maximum Q -factor can be realized for particles with a shape slightly different from spherical.

In [61], the eigenfrequencies and Q -factors of the spheroidal resonator modes were found numerically by solving the Muller boundary integral equations discretized with the Nystrom method. In [61], a determinant was found to search for eigenmode frequencies and, with its help, the resonant frequencies and quality factors of usual eigenmodes of a dielectric spheroid with semi-axes a (along the axis of symmetry) and b (perpendicular to the axis) were found. It was assumed that the spheroid had a volume equal to the volume of a sphere of radius R , and its surface is described by

the equation

$$\left(\frac{\rho}{b}\right)^2 + \left(\frac{z}{a}\right)^2 = 1, \quad a = Rt^{2/3}, \quad b = Rt^{-1/3}, \quad (54)$$

where $t = a/b$. For $t < 1$, we have an oblate spheroid, and for $t > 1$, it is prolate.

Figure 15 shows the dependences of the quality factors of the lowest modes for spheroids with $\varepsilon = 38$ on the aspect ratio of the semi-axes. From Fig. 15, one can draw extremely important and highly nontrivial conclusions that:

- TM modes have significantly higher quality factors than TE modes, due to the fact that they are confined modes (see (26) and (28));

- the quality factors of the lower TM modes (TM_{101} , TM_{201}) are maximal, not for spheres, but for oblate spheroids. Higher-order modes have maximal Q -factors for spheres in accordance with the results of [123];

- the quality factors of all TE modes are maximal for spheres, but not for oblate or prolate spheroids, which also agrees with the results of [123];

- TM_{101} (electric dipole) and TE_{101} (magnetic dipole) mode resonances have good overlap for oblate spheroids ($a/b < 1$). This circumstance was used in [124] to maximize forward scattering by an oblate dielectric spheroid.

A more detailed study of the relationship between the real and imaginary parts of resonant frequencies was carried out in [125] using simulations with COMSOL Multiphysics [78]. Figure 16 shows how the real and imaginary parts of the

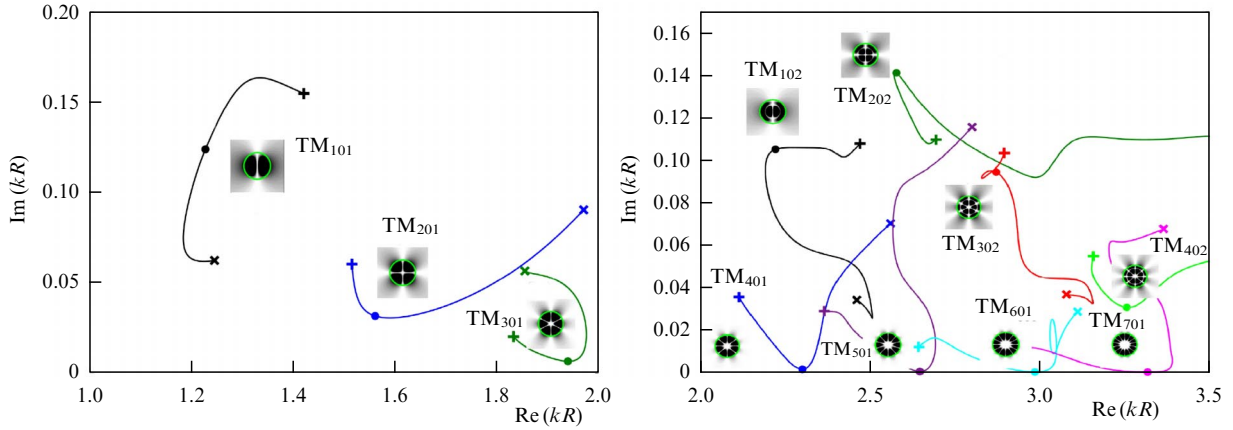


Figure 16. Dependence of real and imaginary parts of resonant frequencies of axisymmetric TM_{nm} modes on the shape of a silicon spheroid with $\epsilon = 12$. Markers ‘ \times ’, ‘+’, and ‘ \bullet ’ on the curve correspond to the oblate spheroid ($a/b = 0.4$), the prolate spheroid ($a/b = 1.6$), and the sphere ($a/b = 1$), respectively. Insets show the distributions of H_ϕ fields in the modes; numbers above insets show orbital and radial quantum numbers of the mode. R is the radius of a sphere with a volume equal to that of the spheroid. (Adapted from [125].)

resonant frequency of a silicon spheroid change depending on the aspect ratio a/b of the spheroids. It can be seen from Fig. 16 that the trajectories of natural frequencies in the complex plane when the shape of the spheroid changes are quite complex, especially in the case of higher modes. Nevertheless, again, high- Q modes without zeros in the radial direction (TM_{301} , TM_{401} , TM_{501} , TM_{601} , TM_{701}) have a near-zero imaginary part of the frequency and, therefore, the maximal Q -factor in the case of a spherical nanoparticle. The low- Q TM_{101} mode has the maximal Q -factor for oblate spheroids, agreeing with the results of [61] (see Fig. 15). In [125], similar results were also obtained for TE modes in spheroids.

4.2.2 Perfect nonradiating modes. Perfect nonradiating modes are not a feature of spherical geometry and definitely exist for axisymmetric bodies of an arbitrary shape. In [40], by expanding the solutions of Eqns (14), (15) in terms of radial $S_{n1}(c, \xi)$ and angular $PS_{n1}(c, \eta)$ spheroidal wave functions [122], it was shown rigorously that perfect modes exist for arbitrary spheroids, and their eigenfunctions and frequencies were found.

The dispersion equation describing perfect nonradiating modes for prolate spheroids with permittivity ϵ has the form [40]

$$\begin{aligned} \text{Det } M &= 0, \\ M_{np} &= \Pi_{np}(c_1, c_0) (\epsilon SD_{p1}(c_0, \xi_0) S_{n1}(c_1, \xi_0) \\ &\quad - S_{p1}(c_0, \xi_0) SD_{n1}(c_1, \xi_0)), \end{aligned} \quad (55)$$

where

$$\begin{aligned} \Pi_{n,p}(c_1, c_0) &= \int_{-1}^1 d\eta PS_{n1}(c_1, \eta) PS_{p1}(c_0, \eta), \\ SD_{n1}(c, \xi_0) &= \frac{\partial(\xi_0^2 - 1)^{1/2} S_{p1}(c, \xi_0)}{\partial \xi_0}, \end{aligned} \quad (56)$$

$$\xi_0 = \frac{t}{\sqrt{t^2 - 1}}, \quad c_0 = \frac{k_0 R \sqrt{t^2 - 1}}{t^{1/3}}, \quad c_1 = \frac{k_0 R \sqrt{\epsilon} \sqrt{t^2 - 1}}{t^{1/3}}.$$

In (56), $k_0 = \omega/c$ and R is the radius of the sphere, which defines the fixed volume of the spheroid. Dispersion equation

(55) is also valid for an oblate spheroid after the corresponding analytic continuation.

We emphasize once again that the fields of perfect nonradiating modes found in [40] are not equal to zero outside the spheroidal resonator, that is, they are not ‘anapole current distributions’ with the field equal to zero outside the resonator. It is also important that perfect nonradiating modes exist for any shape of a spheroid.

The found perfect nonradiating modes of spheroids are not abstract solutions either; they are of great importance for finding the conditions under which the scattered power becomes minimal or even zero. To demonstrate the practical importance of perfect nonradiating modes, the characteristics of scattering of an axisymmetric Bessel beam

$$H_\phi \sim J_1(k_0 \rho \sin \beta) \cos(k_0 z \cos \beta) \quad (57)$$

by spheroidal resonators of various shapes were calculated in [40].

Figure 17 shows the dependence of the scattered power, the energy stored in the spheroid, and the quality factor on the size parameter of nanospheroids with $a/b = 0.7$. It can be

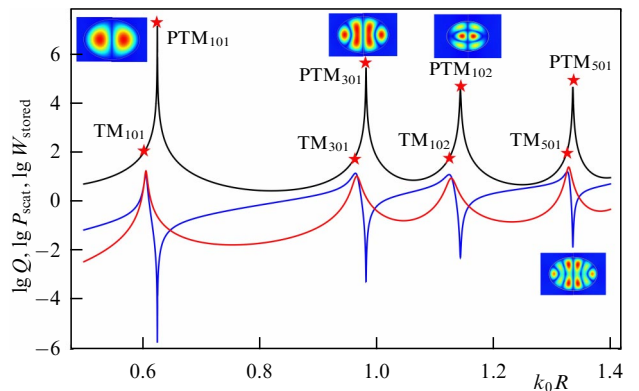


Figure 17. Dependence of scattered power (blue curve), stored energy (red curve (3)), and quality factor (black curve) on the size parameter of nanoparticles. TM symmetric excitation (57) with $\beta = \pi/4$, $\epsilon = 50$, $a/b = 0.7$. All maxima of the Q -factor correspond to perfect nonradiating modes. Asterisks indicate Q -factors of usual modes (TM_{101} , TM_{301} , TM_{501}) and perfect nonradiating modes (PTM_{101} , PTM_{301} , PTM_{501}) [40].

Table 1. Characteristics of some high-quality modes of cylindrical nanoresonators and values of index P (see (28)) that determines the dependence of their quality factors on the refractive index [75].

Mode	Field structure inside the resonator	Far field structure	Multipole orientation	Index P
TE _{01δ}	$H_z = J_0(hr) \cos \beta z$ $E_z = 0$	Magnetic dipole	∥ axis	1.27
HE _{11δ}	$E_z = J_1(hr) \cos \beta z \exp(i\varphi)$ $H_z = 0$	Magnetic dipole	⊥ axis	1.30
HE _{21δ}	$E_z = J_2(hr) \cos \beta z \exp(i2\varphi)$ $H_z = 0$	Magnetic quadrupole	⊥ axis	2.49
EH _{11δ}	$H_z = J_1(hr) \cos \beta z \exp(i\varphi)$ $E_z = 0$	Electric dipole	⊥ axis	2.71
TE _{011+δ}	$H_z = J_0(hr) \sin \beta z$ $E_z = 0$	Magnetic quadrupole	∥ axis	2.38

seen from this figure that, under such excitation, all scattering minima and Q -factor maxima ($Q > 10^5$) are due to the perfect nonradiating modes. The positions of these modes correspond exactly to the solutions of dispersion equation (55). The finite quality factor of the perfect modes (which are infinite in theory) is due to the fact that there is a continuum of usual quasi-normal modes that result in small but finite radiation, which can be reduced unlimitedly by the optimal tuning of the beam. In any case, the power scattered by perfect nonradiating modes (PTM₁₀₁ and PTM₃₀₁) is 4 to 5 orders of magnitude less than that scattered by usual quasi-normal modes (TM₁₀₁ and TM₃₀₁). Accordingly, the quality factors of perfect nonradiating modes are 4–5 orders of magnitude greater than the quality factors of usual modes.

The existence of TE perfect nonradiative modes in spheroids was also theoretically demonstrated in [40].

4.3 Dielectric nanoresonators of more complex shapes

4.3.1 Usual modes of finite-height cylinders. Relatively simple shapes of the resonators considered above can be described theoretically in detail and, consequently, the physics of processes in such nanoresonators is quite understandable. However, from a technological point of view, such resonators are difficult to implement, especially in optical integrated circuits. Therefore, in recent years, special attention has been paid to the study of cylindrical dielectric nanoresonators, that

is, resonators with an external size smaller than the wavelength in the air.

For circular cylindrical resonators of finite height, a great deal of theoretical and experimental research has been done, and therefore their characteristics are generally well known. In particular, Table 1 [75] lists the characteristics of some high- Q modes of cylindrical nanoresonators and the values of the index P (see (28)) that determines their Q -factor as a function of the refractive index. In the same study, one can find corrections related to the shape of a particular cylinder.

For example, for the mode EH_{11δ} (electric dipole perpendicular to the axis), index $P = 2.71$, and this gives the value of the quality factor $Q = 1.4 \times 10^5$ at $\varepsilon = 80$.

A similar study was carried out in [126], where approximation formulas were also found for the eigenfrequencies and quality factors of several principal modes of dielectric cylindrical nanoresonators. In particular, for TM_{01δ} (electric dipole along the axis), the approximation expression for the quality factor is

$$\begin{aligned}
 Q_{\text{TM}_{01\delta}} &= 0.008721\varepsilon^{0.888413} \exp(0.0397475\varepsilon_r) \\
 &\times \left\{ 1 - \left(0.3 - 0.2 \frac{a}{h} \right) \frac{38 - \varepsilon}{28} \right\} \\
 &\times \left\{ 9.498196 \frac{a}{h} + 2058.33 \left(\frac{a}{h} \right)^{4.322261} \exp \left(-3.50099 \frac{a}{h} \right) \right\}.
 \end{aligned} \tag{58}$$

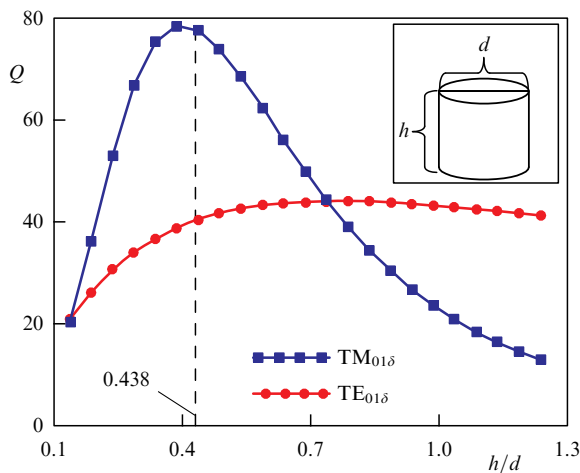


Figure 18. Dependence of Q -factors of the lowest TE_{01δ} and TM_{01δ} modes in a cylindrical resonator with $\varepsilon = 38$ as a function of aspect ratio h/d [61, 127].

Figure 18 shows the Q -factors of the lowest TE_{01δ} and TM_{01δ} modes in a cylindrical resonator with $\varepsilon = 38$ [61, 127].

4.3.2 Supercavity modes in cylinders. Recently, much attention has gone to the theoretical and experimental study of high-quality modes in cylindrical nanoresonators [21, 25, 30, 37, 38, 128]. In view of the high-quality factor, these, in general, usual quasi-normal modes have even been called ‘supercavity’ modes or ‘quasi-BIC states.’ These modes arise at optimal cylinder shapes, at which the lowest spherical harmonic disappears in the multipole expansion of the eigenmode (18).

In [69], modes were studied in a more complex cylinder of finite height with an equilateral triangle at the base. In view of the presence of sharp corners, it is difficult to expect the presence of high-quality modes in such resonators in the general case. However, at certain parameters, there are modes (sometimes also called ‘supercavity’ modes) that do not sense

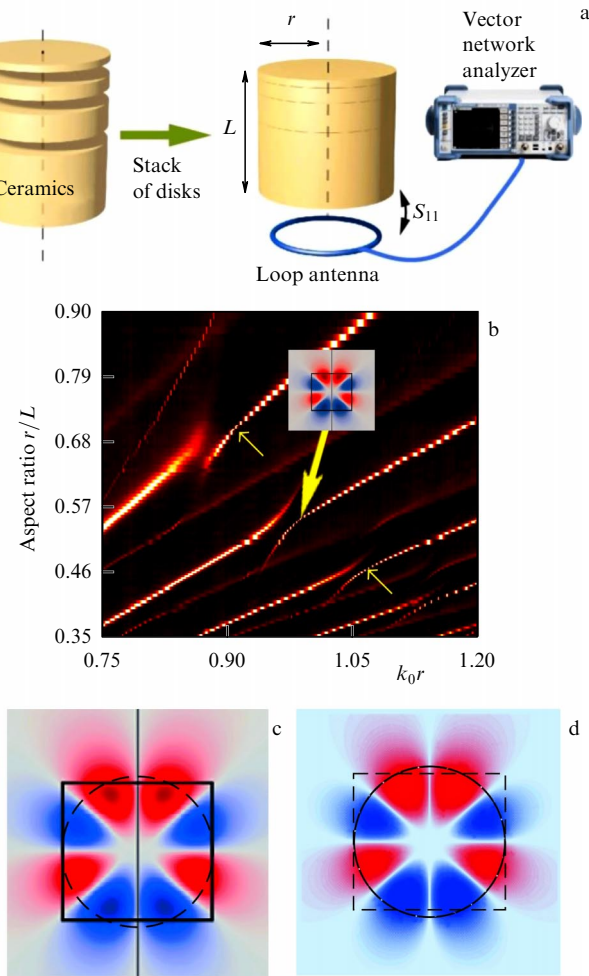


Figure 19. Experimental observation of ‘supercavity’ modes in subwavelength cylindrical resonators. (a) Experimental setup for measuring scattering in the radio frequency range. Resonator consists of several ceramic disks of different heights combined in a single cylinder with radius $r = 15.7$ mm, dielectric constant $\epsilon = 44.8$, and ceramic loss tangent of about $\tan \delta = 10^{-4}$. TE modes of the resonator are excited by a loop antenna connected to a vector network analyzer. (b) Dependence of the experimentally measured scattering coefficient $1 - |S_{11}|$ on the size parameter k_0r and the aspect ratio r/L . Arrows show the positions of the ‘supercavity’ modes and the spatial structure of one of them (adapted from [38]). Comparison of the structures of (c) the ‘supercavity’ mode in a cylinder ($\epsilon = 44.8$, $Q = 180,000$) and (d) the TE_{401} mode in a sphere ($\epsilon = 44.8$, $Q = 214,000$).

sharp corners, and their quality factors approach those of smoother resonators of the same volume, such as spheres or spheroids (see Section 4.2).

In [38], an experimental observation of ‘supercavity’ modes in subwavelength ceramic resonators in the radio frequency range was carried out. Figure 19 shows the experimental setup and the results of measuring the scattering coefficient.

Mathematical analyses of the measured scattering coefficients showed that, by fine-tuning the shape of the resonator, in the experiment it is possible to achieve a substantial increase in the quality factor, reaching values up to $Q_{\text{super}} = 1.25 \times 10^4$ for a mode in ceramics with a loss tangent of about 10^{-4} . Direct finite element simulation shows that the intrinsic radiation Q -factor of the cylinder mode is about $Q_{\text{super}} = 180,000$, approaching the Q -factor of the TE_{401} mode in a

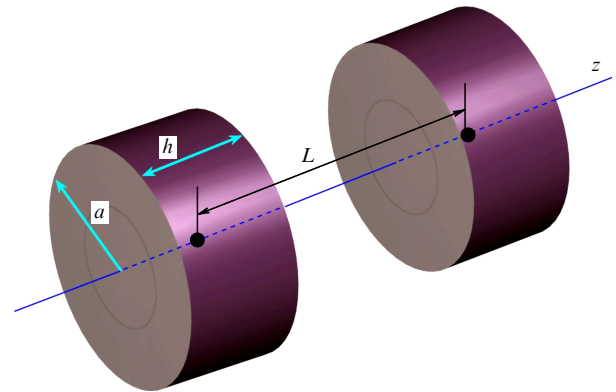


Figure 20. Geometry of the problem of ‘supercavity’ modes in a system of two coaxial silicon cylinders.

sphere with the same permittivity and the same volume, $Q_{\text{sph}} = 213,945$, $k_0r = 1.04$.

Figure 19c shows that the spatial structure of the ‘supercavity’ mode is close to the structure of the field in a spherical resonator, and the cylinder edges are in the region of a small field, explaining the absence of scattering by them and the high-quality factor of these modes. ‘Supercavity’ modes have a Q -factor lower than those of modes of a similar structure in spheres of the same material and the same volume, in full agreement with the results of [123] (see Section 4.2.1).

A system similar to that shown in Fig. 19a was also studied in [129] to see if it could achieve super scattering [130–132] rather than the maximal quality factor. By optimizing the relationship between the spherical multipole content of the excited mode, it was shown in [129] that the optimized structures in the limit of dipole scattering have a scattering cross section that exceeds the limit for a sphere by a factor of 4.

‘Supercavity’ modes in a system of two coaxial silicon cylinders (Fig. 20) were analyzed in detail in [133] using simulations with COMSOL Multiphysics [78].

The physics of this problem is much richer than the physics of a single cylinder, since an additional parameter L —the distance between the centers of the cylinders—appears. Figure 21 shows the evolution of the resonant frequencies of axisymmetric TE modes in the complex plane as a function of the distance L between the cylinders. Again, this figure shows that the minimum imaginary part of the frequency occurs at $L = 1.75h$ on the curve corresponding to antisymmetrical hybridization. In this case, the quality factor $Q = 5500$, and the field structure is close to that of the TE_{602} mode in the sphere. Another high-quality mode appears at $L = 1.08h$ on the curve corresponding to symmetrical hybridization. The structure of this mode is close to that of the TE_{502} mode in a sphere, and the quality factor is lower than in the case of antisymmetrical hybridization at $L = 1.75h$.

An interesting approach to the creation of high- Q optical nanoresonators was proposed in [23], where it was shown that a cavity in a spherical or cylindrical resonator can significantly reduce the fraction of lower spherical harmonics, since they are localized closer to the resonator center and the cavity acts as a filter of lower harmonics. It is important that the contribution of electric multipoles decrease especially strongly. This interesting result

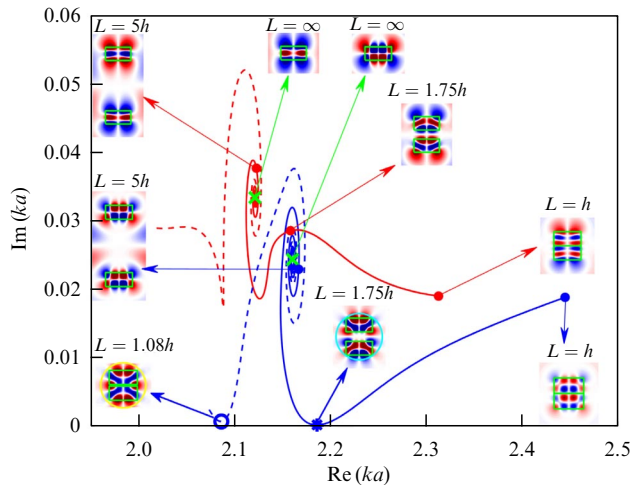


Figure 21. Evolution of resonant frequencies of axisymmetric TE modes in the complex plane as a function of distance between the centers of the cylinders L . Positions of resonant frequencies of an isolated cylinder ($L = \infty$) are shown by green \times 's. Trajectories of antisymmetric and symmetric modes beginning from point $L = \infty$ are shown by solid and dashed lines. $a = 0.5 \mu\text{m}$, $a/h = 0.96$. Insets show distribution E_φ and corresponding distance L between cylinders [133].

was confirmed experimentally with silicon nanorings (see also Fig. 1).

In general, it can be said that ‘supercavity’ modes in circular cylinders are a special case of the well-studied quasi-normal modes [75, 126]. ‘Supercavity’ modes are close in structure and Q -factor to the modes of spherical resonators of the same volume and with the same permittivity, which have the highest possible quality factors [123, 134].

4.3.3 Perfect modes in a cylindrical nanoresonator. In a cylindrical resonator, for any aspect ratios (and not only for exceptional ones, as in the case of ‘supercavity’ modes), in addition to the usual modes, there are also perfect nonradiating modes [40, 41].

In [135], scattering spectra in a system based on a silicon dielectric cylinder were studied experimentally using highly focused axisymmetric Bessel beams with radial and azimuthal polarizations (Fig 22). In this study, due to the use of such polarizations, it was possible to demonstrate almost complete suppression of scattering from the Si nanodisk. Figure 23 shows the scattered power spectrum for different polarizations.

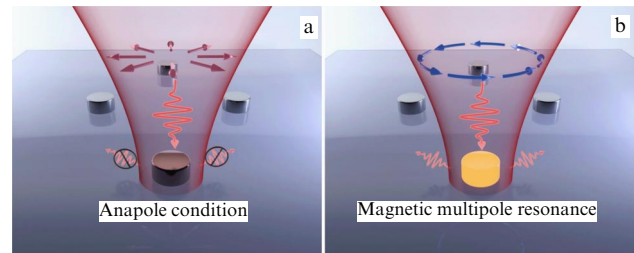


Figure 22. Excitation of an Si disk by strongly focused beams with radial (a) and azimuthal (b) polarizations [135].

It can be seen from Fig. 23 that, for radial polarization at $\lambda = 720 \text{ nm}$, the scattered power practically disappears. Another interesting feature of this geometry is that the same sample, when irradiated with an azimuthally polarized beam, strongly radiates a magnetic quadrupole spherical harmonic.

The authors of [135] call the disappearance of scattering at $\lambda = 720 \text{ nm}$ the ‘anapole condition,’ but the connection of this condition with natural oscillations of the resonator is not discussed, and the ‘anapole condition’ can correspond both to weak radiation of high-quality ‘supercavity’ modes and to the excitation of the perfect nonradiating modes considered above [40].

The question of the existence of perfect nonradiating modes in finite-height cylinders of noncircular cross section is still open. However, perfect modes always exist for straight infinite cylinders of arbitrary cross section [41].

5. Modes in nanoresonators made of metamaterials

The history of metamaterials begins with a paper in *Physics–Uspekhi* [136], in which V G Veselago showed that, unlike metals, matter (then hypothetical) with both negative permittivity and permeability allows the propagation of waves with a negative refractive index, $n = -\sqrt{\epsilon\mu}$, that is, with oppositely directed phase and group velocities of waves.

The rapid development of this area began with studies [137, 138], where metamaterials with a negative refractive index were realized in the microwave frequency range. Later, metamaterials were implemented in the IR and visible ranges (for more details, see, for example, [139–141]). Such materials are now called NIMs (Negative Index Materials) or DNG (double negative) metamaterials. Then, all substances with unusual properties began to be called metamaterials, for

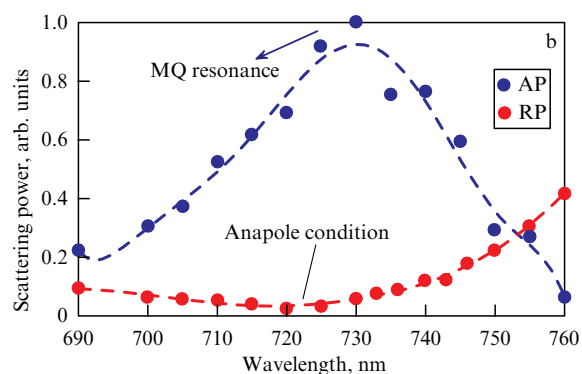
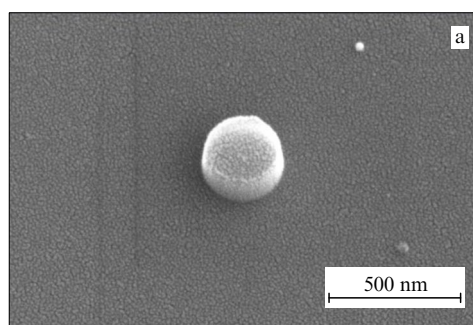


Figure 23. (a) SEM image of an Si nanoresonator ($r = 150 \text{ nm}$, $h = 160 \text{ nm}$) on an SiO_2 substrate. (b) Scattered power spectrum for different polarizations of the excitation beam [135].

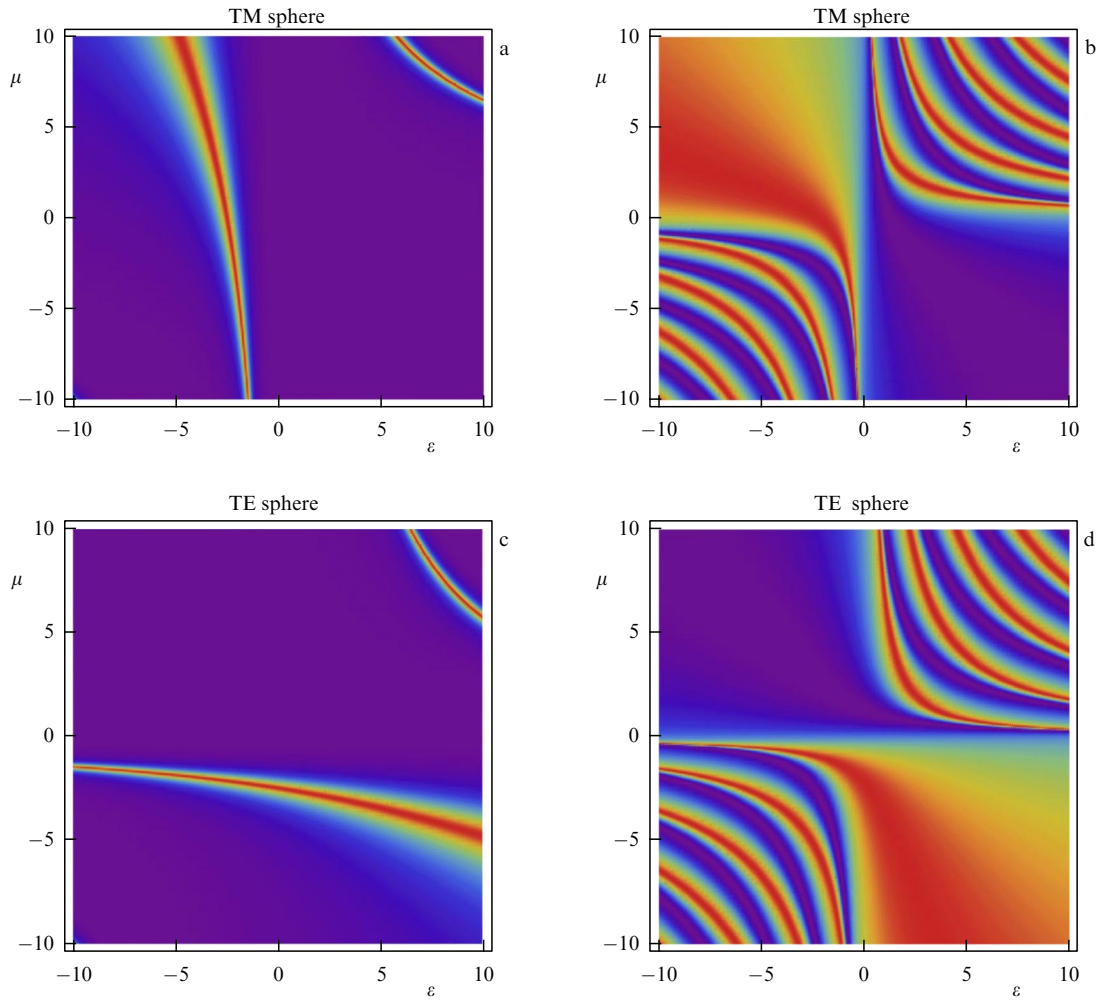


Figure 24. Dependences of amplitudes of Mie scattering coefficients depending on permittivity and permeability. (a, b) $|q_1|$ (TM modes) for size parameter $ka = 0.5, ka = 1.5$, (c, d) $|p_1|$ (TE modes) for size parameter $ka = 0.5, ka = 1.5$. In these figures, the upper right quadrant corresponds to usual dielectrics, while the lower left quadrant corresponds to a sphere with a negative refractive index [1, 142].

example, chiral metamaterials, hyperbolic metamaterials, or metamaterials with a permittivity near zero (ENZ, epsilon near zero, or ZIM, zero-index metamaterials).

5.1 Modes in a sphere with a negative refractive index

In [1, 142], the Mie theory was directly applied to describe the optical properties of a nanoresonator made of a metamaterial with a negative refractive index. Figure 24 shows the dependences of the amplitudes of the Mie scattering coefficients (33) and (34) as a function of permittivity and permeability.

From Fig. 24, it can be seen that the resonant properties of a sphere with a negative refractive index are only partially similar to those of a usual dielectric sphere. In it, along with the usual bulk modes, there are also surface LH (left-handed) modes, which are localized on the surface. Such a complex structure of the Mie coefficients leads to a completely different structure of modes and their quality factors compared to usual dielectric spheres.

Figure 25 shows the dependences of the TE Mie coefficients p_n on the size parameter ka of the sphere. Figure 25 shows clearly the highly anomalous behavior of TE resonances in a sphere made of a DNG metamaterial: with an increase in the mode multipole order, a decrease in

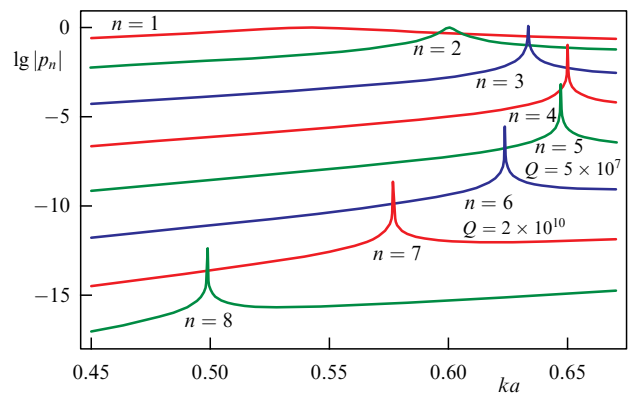


Figure 25. Dependences of TE Mie coefficients $\lg |p_n|$ on size parameter ka of a sphere ($\epsilon = -15, \mu = -1.1, -\sqrt{\epsilon\mu} \approx -4$) [1].

the size parameter of the sphere ka is required to achieve resonance. Moreover, the number of such resonances is finite. A decrease in the size parameter at which high multipole order modes exist leads to the fact that they become surface modes, that is, the field maximum falls on the surface of the sphere.

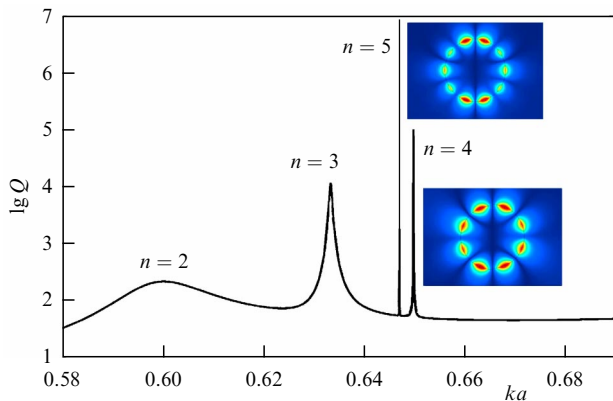


Figure 26. Dependence of the generalized quality factor of TE modes in a sphere with $\varepsilon = -15$, $\mu = -1.1$ on size parameter ka . Quality factors of TE modes are $Q_2 = 107$, $Q_3 = 4125$, $Q_4 = 327,769$, $Q_5 = 5.32372 \times 10^7$. Modes with $n = 6, 7, 8$, clearly visible in Fig. 25, are not visible here due to insufficient graphics resolution. Insets show the distribution of the electric field of TE modes in the cross section of the sphere [142–144].

Figure 26 shows the dependence of the generalized quality factor of a sphere made of DNG metamaterial on the size parameter ka . It can be seen from this figure that, indeed, spheres with a negative refractive index have huge quality factors, which are associated with the surface nature of the LH modes. Their other most important feature is that such huge Q -factors arise for spheres of subwavelength sizes even at relatively small absolute values of the refractive index. Both these features radically distinguish modes in DNG resonators from those in usual dielectric resonators.

5.2 Modes in a chiral sphere

Chiral metamaterials, where the polarization depends on both electric and magnetic fields, are related to DNG metamaterials directly. The material equations of chiral media can be expressed in the form [145, 146]

$$\mathbf{D} = \varepsilon \left(\mathbf{E} + \chi \mathbf{V} \times \frac{\mathbf{E}}{k_0} \right), \quad \mathbf{B} = \mu \left(\mathbf{H} + \chi \mathbf{V} \times \frac{\mathbf{E}}{k_0} \right), \quad (59)$$

where χ is the dimensionless chirality parameter. In bi-isotropic chiral metamaterials, where ε , μ , and χ are scalar quantities, the wave vectors (k_L, k_R) and the refractive indices (n_L, n_R) for right and circularly polarized waves have different values:

$$k_L = k_0 \frac{\sqrt{\varepsilon\mu}}{1 - \chi\sqrt{\varepsilon\mu}} = k_0 n_L, \quad k_R = k_0 \frac{\sqrt{\varepsilon\mu}}{1 + \chi\sqrt{\varepsilon\mu}} = k_0 n_R. \quad (60)$$

It can be seen from expressions (60) that, for a sufficiently large $\chi\sqrt{\varepsilon\mu}$, one of the refractive indices (n_R or n_L) will necessarily become negative. In [147], it was proposed to use this fact to realize media with a negative refractive index. Chiral media can be made in several ways [148–152]. Figure 27 shows possible realizations of a chiral spherical nanoresonator.

It was shown in [153, 154] within the framework of the quasi-static approximation that, instead of a dipole plasmon resonance, $\varepsilon(\omega) + 2 = 0$, a chiral-plasmon dipole resonance arises in chiral spheres, the condition for which is

$$(\varepsilon + 2)(\mu + 2) = 4\varepsilon\mu\chi^2. \quad (61)$$

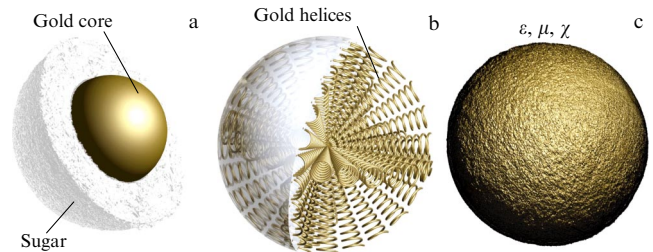


Figure 27. Possible realizations of a chiral sphere: (a) gold nanosphere covered with a shell of sugar; (b) radial spirals forming a sphere; (c) effective description of a chiral nanoparticle.

A complete electrodynamic theory of resonances in chiral spherical nanoparticles of arbitrary sizes was developed in [155–157], where expressions for analogues of the Mie coefficients were found. These expressions are much more complicated, since in chiral spheres it is no longer possible to separate them into TE and TM modes. However, it is possible to introduce more complex modes, called in [156] A and B type modes. Figure 28 shows the dependence of the scattering coefficient T_4^A (type A mode), which reduces to the Mie coefficient for TM mode scattering, q_4 , at $\chi = 0$, on the permittivity ε and permeability μ for various values of the size parameter $k_0 a$ and chirality χ . It can be seen from this figure that the structure of the modes of the chiral sphere is much more complicated than in the case of the DNG sphere, since here the chiral-plasmon resonance (61) arises additionally, manifesting itself in a discontinuity in the dispersion curve of the surface DNG modes.

The dispersion equation that determines the eigenfrequencies of the chiral sphere has the form [155, 156]

$$\Delta_n = W_n(L)V_n(R) + W_n(R)V_n(L) = 0,$$

$$W_n(J) = \left(\frac{\varepsilon}{\mu} \right)^{1/2} \psi_n(k_J a) \zeta_n^{(1)'}(k_0 a) - \psi_n'(k_J a) \zeta_n^{(1)}(k_0 a), \quad (62)$$

$$V_n(J) = \psi_n(k_J a) \zeta_n^{(1)'}(k_0 a) - \left(\frac{\varepsilon}{\mu} \right)^{1/2} \psi_n'(k_J a) \zeta_n^{(1)}(k_0 a),$$

where $\psi_n(z) = z j_n(z)$ and $\zeta_n^{(1)}(z) = z h_n^{(1)}(z)$ are the Riccati–Bessel functions, the prime denotes the derivative, and index J takes the values L, R (see (60)). It is important that, as in a usual dielectric sphere, the expression for the determinant Δ_n does not depend on the azimuthal quantum number m . Figure 29 shows the projection of the dependence of the eigenfrequencies of chiral sphere with $\varepsilon = 2 + 0.04i$ on χ , $\text{Re}(k_0 a)$, $\text{Im}(k_0 a)$ onto the $(\text{Re}(k_0 a), \text{Im}(k_0 a))$ plane for an orbital quantum number $n = 1$. It can be seen from this figure that an increase in chirality (moving downwards along the curves) leads to a significant increase in the quality factor of natural oscillations. This is mainly due to the fact that the wave number of one of the polarizations in a chiral medium can increase infinitely (the pole in (60)), and therefore the wavelength of such waves in a sphere is much smaller than in vacuum, leading to an effective increase in the size of the sphere and the quality factor of the modes existing in it.

Figure 30 shows the distribution of the z -component of the electric field in the plane $z = 0$ (shaded plane in the geometry inset) for different values of the dimensionless chirality parameter corresponding to different values of the radial quantum number $\nu = 1, 2, 3, 4$ when the sphere is excited by a plane wave.

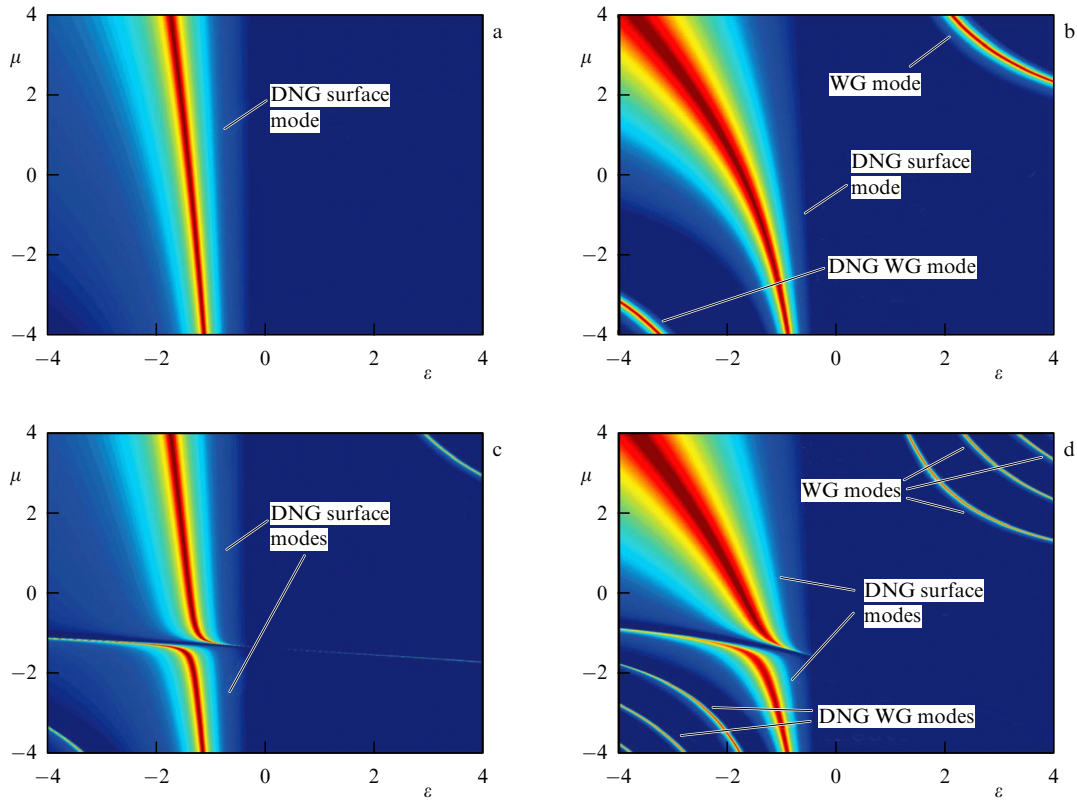


Figure 28. Dependence of absolute values of the scattering coefficient of A modes, T_4^A , of a chiral spherical particle on permittivity ϵ and permeability μ for various values of the parameters: (a) $\chi = 0, k_0a = 1.5$; (b) $\chi = 0, k_0a = 2.5$; (c) $\chi = 0.1, k_0a = 1.5$; (d) $\chi = 0.1, k_0a = 2.5$. Nanosphere is located in vacuum [156].

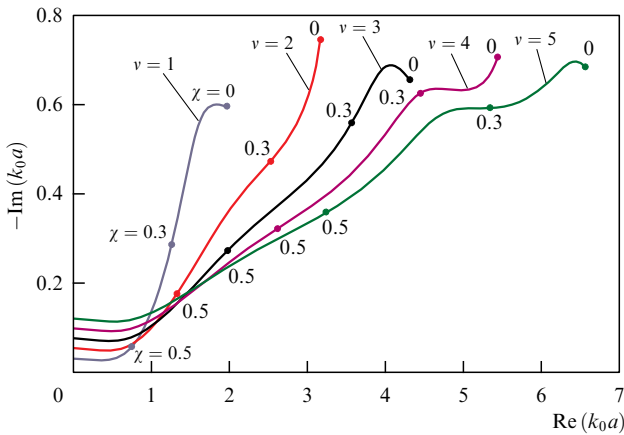


Figure 29. Projection of the dependence of eigenfrequencies of a chiral sphere with $\epsilon = 2 + 0.04i$ on $\chi, \text{Re}(k_0a), \text{Im}(k_0a)$ onto the $(\text{Re}(k_0a), \text{Im}(k_0a))$ plane for orbital quantum number $n = 1$. Different colors of the curves correspond to different radial quantum numbers $v = 1-5$. Colored labels near points indicate chirality parameter χ at that point (3rd coordinate) [157].

Other regimes of eigen oscillations for a chiral sphere were considered in [156–158]. Natural oscillations in a cluster of chiral spheres [159] and in a chiral sphere with an asymmetric shell [160] were also studied in detail.

5.3 Modes in a sphere made of a hyperbolic metamaterial

In [161], modes were considered in a spherical nanoresonator made of a hyperbolic metamaterial (HMM), that is, an anisotropic material where the diagonal values

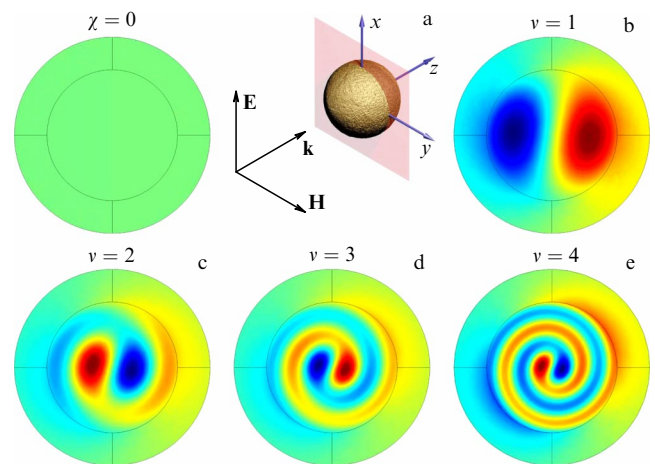


Figure 30. Geometry of the problem of the scattering of a plane wave with a $\lambda = 570\text{-nm}$ chiral sphere $\epsilon = 2 + 0.04i$ and $a = 70\text{ nm}$ and spatial distribution of the z -component of electric field E_z in the $z = 0$ plane (shaded plane in geometry inset) for different values of the dimensionless chirality parameter corresponding to different values of radial quantum number $v = 1$ ($\chi \approx 0.5$), $v = 2$ ($\chi \approx 0.6$), $v = 3$ ($\chi \approx 0.65$), $v = 4$ ($\chi \approx 0.67$), eigenmodes with $n = 1, m = 1$. Case $\chi = 0$ is also presented for comparison.

of the permittivity tensor have different signs [162] (Fig. 31a).

As is known [162], the key feature of the HMM is the possibility of the existence of propagating waves with an unlimited radial wave number (Fig. 31b), enabling the existence of resonant modes in spheres of arbitrarily small

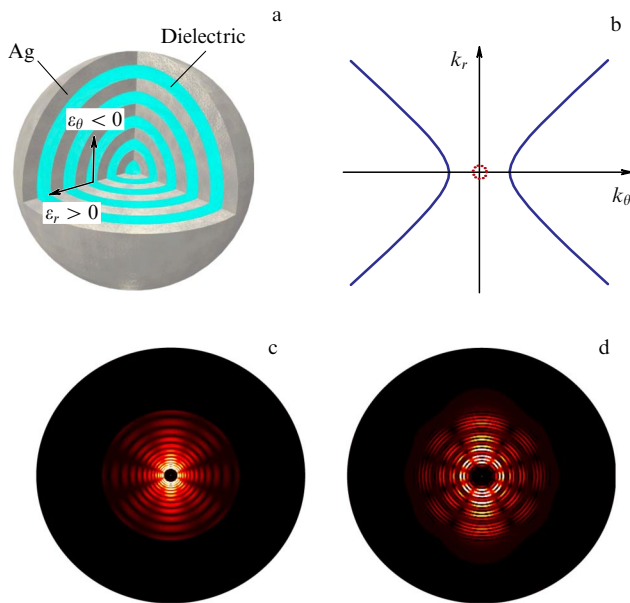


Figure 31. (a) Geometry of a hyperbolic resonator consisting of alternating metal and dielectric layers. (b) HMM isofrequency contour in momentum space calculated in the effective medium approximation with $\lambda = 1000$ nm. Small dotted circle in the center represents the isofrequency contour in vacuum at the same wavelength. (c) Field distribution in the TM resonator mode with orbital number $n = 4$ in a homogeneous hyperbolic resonator and in a multilayer structure (d). In (c), the HMM resonator has an inner radius of 20 nm and outer radius of 200 nm and resonant wavelength $\lambda = 992$ nm. HMM resonator in (d) consists of 20 functional layers, each 10 nm thick; resonant wavelength in (d) is $\lambda = 977$ nm [161].

sizes (in the approximation of a homogeneous medium, of course) (Fig. 31c,d). With a decrease in the outer radius of resonator R , the Q -factors of the modes increase unlimitedly, according to the law $Q_{\text{rad}} \propto R^{-(2n+1)}$, where n is the order of the multipole moment of the mode. Although the authors of Ref. [161] say that the high- Q modes found by them can be attributed to whispering gallery modes, this is apparently not the case, and it can be seen from Fig. 31c,d that these modes are concentrated at the center of the resonator. From a mathematical point of view, this is because the radial distributions of TM fields inside a spherical HMM resonator are described not by usual Bessel functions of a half-integer order but by Bessel functions with an imaginary order [163],

$$J_{l+1/2}(\sqrt{\epsilon} k_0 r) \Rightarrow J_{g(l)+1/2}(\sqrt{\epsilon_\theta} k_0 r), \quad (63)$$

where the imaginary order is given by

$$g(l) + \frac{1}{2} = \frac{1}{2} \sqrt{1 + 4 \frac{l(l+1)\epsilon_\theta}{\epsilon_r}}. \quad (64)$$

Bessel functions with an imaginary order do not tend to zero at the origin, leading to the concentration of fields at the center of the sphere.

The properties of HMM resonators are generally similar to those of resonators made of DNG or chiral metamaterials: in all cases, modes can exist for arbitrarily small external dimensions of the resonators. From a physical point of view, these resonators are fundamentally different: in nanoresonators made of hyperbolic and chiral metamaterials, the modes are bulk, while in DNG nanoresonators, superhigh- Q modes are of a surface nature.

6. Examples of possible applications of optical nanoresonators

Although optical nanoresonators have very interesting fundamental properties, their wide practical application is yet to come. Nevertheless, the principles of operation of several optical nanodevices based on the resonant properties of nanoparticles have already been experimentally demonstrated.

(1) First of all, attempts to create sources of coherent radiation with the use of optical nanoresonators should be noted. In this regard, first of all, it is worth mentioning spasers and nanolasers, based on plasmonic nanoresonators [2, 4] and on dielectric nanoresonators [22, 25, 26, 164]. There are also proposals to use HMM nanoresonators for nanolasers [165].

(2) Optical nanoresonators can also be used effectively to control the spontaneous emission of elementary quantum systems [143, 144, 166–172] and to construct bright artificial fluorophores [91] and quantum photonic circuits [173] on this basis (where a 1D photonic crystal nanoresonator was used).

(3) An important area of application of optical nanoresonators is to increase the efficiency of solar cells, and, for this purpose, not only plasmonic but also dielectric nanoresonators are used [174–178].

(4) The high sensitivity of natural oscillations in optical nanoresonators to the refractive index of the environment makes it possible to create highly sensitive biosensors on this basis [110, 179–185].

(5) The high field concentration in high- Q modes of optical nanoresonators and the correct choice of pump polarization increase the efficiency of the generation of the second [21, 28, 188, 189] and the third [27, 190–192] harmonics and other nonlinear effects [17, 21, 29] significantly (by 2 orders of magnitude compared to the best microresonators [186, 187]).

(6) Electromagnetic resonances in dielectric nanoresonators can be used to implement optical magnetism ($\mu \neq 1$) [120, 193, 194].

7. Conclusion

The review presents the current state of a rapidly developing field of optics: the optics of 3D nanoresonators, that is, resonators with subwavelength dimensions in all directions. In this case, the focus is on the fundamental aspects of describing the optical properties of such nanoresonators. The rapid development of this area by the efforts of various scientific groups led to the discovery of several new effects and to the emergence of colorful new terms related to them, which are often not precisely defined. This complicates the further development of this field, and we try to connect the new terms with each other and with generally accepted definitions.

Mainly, the review considers highly symmetric nanoresonators without internal losses, which have ultra high Q -factors at resonant frequencies. However, a whole class of nanoresonators — asymmetric nanoresonators — remains outside the scope of the review. It is difficult to expect superhigh quality factors in the usual sense of the word from such resonators, but interesting nonstationary field distributions can be realized in them, which can serve as the basis for information processing on a single chip and other applications. Super scattering regimes can also exist in asymmetric nanoresonators.

The materials of nanoresonators have a fundamentally important effect on their properties, and therefore both plasmonic and dielectric nanoresonators are considered in the review. The review also considers nanoresonators made from hypothetical metamaterials. Although these metamaterials have not yet been realized on the nanoscale (see, however, [195]), the extreme properties of resonators made from them make the search for such metamaterials extremely topical.

In the review, modes of natural oscillations are considered in more or less detail, but the methods for their effective excitation are only outlined. At present, optical nanoresonators are mainly excited by an external (far) field, and, therefore, studies aimed at creating far-field configurations that effectively interact with eigenfields are extremely important. Especially interesting for the excitation of symmetrical nanoresonators are Bessel beams with a certain (radial or azimuthal) polarization. For example, only the use of an azimuthally polarized beam, not a linearly polarized one, makes it possible to increase the efficiency of the second harmonic generation by 2 orders of magnitude [28]. Even more important from a practical point of view is the excitation of natural oscillations in nanoresonators using near fields for the construction of photonic nanochips. It is natural to consider elementary quantum systems (dye molecules or quantum dots) to be the sources of near fields. Such studies are just beginning, and mostly in theory, since the experiments are very complex.

We believe that fruitful achievements and great breakthroughs will be made in this area in the future, and we hope that this review will give an additional impetus to research in this direction.

Acknowledgments

The study was funded by the Russian Foundation for Basic Research, project number 20-12-50136.

References

- Klimov V V *Nanoplasmonics* (Singapore: Pan Stanford Publ., 2014)
- Noginov M A et al. *Nature* **460** 1110 (2009)
- Ge D et al. *Nat. Commun.* **11** 3414 (2020)
- Kwon S-H et al. *Nano Lett.* **10** 3679 (2010)
- Celebrano M et al. *Nat. Nanotechnol.* **10** 412 (2015)
- Biagioni P, Huang J-S, Hecht B *Rep. Prog. Phys.* **75** 024402 (2012)
- Yang Z-J et al. *Phys. Rep.* **701** 1 (2017)
- Paniagua-Domínguez R et al. *J. Appl. Phys.* **126** 150401 (2019)
- Krasnok A E et al. *JETP Lett.* **94** 593 (2011); *Pis'ma Zh. Eksp. Teor. Fiz.* **94** 635 (2011)
- Krasnok A E et al. *Opt. Express* **20** 20599 (2012)
- Krasnok A E et al. *Phys. Usp.* **56** 539 (2013); *Usp. Fiz. Nauk* **183** 561 (2013)
- Rocco D et al. *J. Opt. Soc. Am. B* **34** 1918 (2017)
- Sinev I et al. *ACS Photon.* **7** 680 (2020)
- Luk'yanchuk B S et al. *ACS Photon.* **2** 993 (2015)
- Manna U et al. *J. Appl. Phys.* **127** 033101 (2020)
- Baranov D G et al. *Optica* **4** 814 (2017)
- Kivshar Yu *Nat. Sci. Rev.* **5** 144 (2018)
- Koshelev K et al. *Nanophotonics* **8** 725 (2019)
- Yang Y, Bozhevolnyi S I *Nanotechnology* **30** 204001 (2019)
- "Physicists Trap Light in Nanoresonators for Record Time". ITMO News, 17.01.2020, <https://physics.itmo.ru/en/news/physicists-trap-light-nanoresonators-record-time>
- Koshelev K et al. *Science* **367** 288 (2020)
- Tiguntseva E et al. *ACS Nano* **14** 8149 (2020)
- Zenin V A et al. *ACS Photon.* **7** 1067 (2020)
- Melik-Gaykazyan E et al. *Nano Lett.* **21** 1765 (2021)
- Mylnikov V et al. *ACS Nano* **14** 7338 (2020)
- Hwang M-S et al. *Nanophotonics* **10** 3599 (2021)
- Sadrieva Z et al. *Phys. Rev. B* **100** 115303 (2019)
- Bogdanov A A et al. *Adv. Photon.* **1** 016001 (2019)
- Carletti L et al. *Phys. Rev. Res.* **1** 023016 (2019)
- Carletti L et al. *Phys. Rev. Lett.* **121** 33903 (2018)
- Parker J A et al. *Phys. Rev. Lett.* **124** 097402 (2020)
- Luk'yanchuk B et al. *Phys. Rev. A* **95** 063820 (2017)
- Miroshnichenko A E et al. *Nat. Commun.* **6** 8069 (2015)
- Luk'yanchuk B et al. *Philos. Trans. R. Soc. A* **375** 20160069 (2017)
- Baryshnikova K V et al. *Adv. Opt. Mater.* **7** 1801350 (2019)
- Wei L et al. *Optica* **3** 799 (2016)
- Rybin M V et al. *Phys. Rev. Lett.* **119** 243901 (2017)
- Odit M et al. *Adv. Mater.* **33** 2003804 (2021)
- Klimov V *Opt. Lett.* **45** 4300 (2020)
- Klimov V *Photonics* **9** 1005 (2022)
- Klimov V V, Guzatov D V *Photonics* **10** 248 (2023)
- Schwefel H G L et al., in *Optical Microcavities* (Advanced Series in Applied Physics, Vol. 5, Ed. K Vahala) (Singapore: World Scientific, 2004) p. 415, https://doi.org/10.1142/9789812565730_0009
- Jackson J D *Classical Electrodynamics* (New York: Wiley, 1975)
- Courant R, Hilbert D *Methoden der mathematischen Physik* (Berlin: Springer, 1924); Translated into English: *Methods of Mathematical Physics* Vol. 1 (Hoboken, NJ: John Wiley and Sons, 1989); Translated into Russian: *Metody Matematicheskoi Fiziki* Vol. 1 (Moscow-Leningrad: GTTI, 1933)
- de Broglie L *Problèmes de propagations guidées des ondes électromagnétiques* (Paris: Gauthier-Villars, 1941); Translated into Russian: *Elektromagnitnye Volny v Volnovodakh i Polykh Rezonatorakh* (Moscow: GIIL, 1948)
- Weinstein L A *Open Resonators and Open Waveguides* (Boulder, CO: Golem Press, 1969); Translated from Russian: *Otkrytye Rezonatory i Otkrytye Volnovody* (Moscow: Sov. Radio, 1966)
- Richtmyer R D *J. Appl. Phys.* **10** 391 (1939)
- Affolter P, Eliasson B *IEEE Trans. Microwave Theory Tech.* **21** 573 (1973)
- Christopoulos T et al. *Opt. Express* **27** 14505 (2019)
- Wu T, Gurioli M, Lalanne P *ACS Photon.* **8** 1522 (2021)
- Bohren C F, Huffman D R *Absorption and Scattering of Light by Small Particles* (New York: Wiley, 1983)
- Kristensen P T, Van Vlack C, Hughes S *AIP Conf. Proc.* **1398** 100 (2011)
- Kristensen P T, Hughes S *ACS Photon.* **1** 2 (2014)
- Sauvan C et al. *Phys. Rev. Lett.* **110** 237401 (2013)
- Lalanne P et al. *Laser Photon. Rev.* **12** 1700113 (2018)
- Muljarov E A, Langbein W *Phys. Rev. B* **94** 235438 (2016)
- Coccioli R et al. *IEE Proc. Optoelectron.* **145** 391 (1998)
- Doost M B, Langbein W, Muljarov E A *Phys. Rev. A* **87** 043827 (2013)
- Sauvan C *Opt. Express* **29** 8268 (2021)
- Dmitriev V I, Zakharov E V *Metod Integral'nykh Uravnenii v Vychislitel'noi Elektrodinamike* (Method of Integral Equations in Computational Electrodynamics) (Moscow: MAKS Press, 2008)
- Bulygin V S et al. *IET Microwaves Antennas Propag.* **9** 1186 (2015)
- Sukharevsky I O et al. *Opt. Eng.* **58** (1) 016115 (2019)
- Davidovich M V *Izv. Saratov. Univ. Novaya Ser. Ser. Fiz.* **8** (1) 3 (2008) <https://doi.org/10.18500/1817-3020-2008-8-1-3-14>
- Voitovich N N, Katsenelenbaum B Z, Sivov A N *Sov. Phys. Usp.* **19** 337 (1976); *Usp. Fiz. Nauk* **118** 709 (1976)
- Agranovich M S, Katsenelenbaum B Z, Sivov A N, Voitovich N N *Generalized Method of Eigenoscillations in Diffraction Theory* (Berlin: Wiley-VCH, 1999); Translated from Russian: Voitovich N N, Katsenelenbaum B Z, Sivov A N *Obobshchennyi Metod Sobstvennykh Kolebanii v Teorii Difraksii* (Moscow: Nauka, 1977)
- Klimov V V, Ducloy M, Letokhov V S *Quantum Electron.* **31** 569 (2001); *Kvantovaya Elektron.* **31** 569 (2001)
- von Neumann J, Wigner E P *Phys. Z.* **30** 465 (1929)
- Zel'dovich I B *Sov. Phys. JETP* **6** 1184 (1958); *Zh. Eksp. Teor. Fiz.* **33** 1531 (1957)
- Gladyshev S, Frizyuk K, Bogdanov A *Phys. Rev. B* **102** 075103 (2020)
- Wu T et al. *Phys. Rev. A* **101** 011803 (2020)
- Lord Rayleigh F R S *Philos. Mag.* **5** 44 28 (1897)
- Stevenson A F J. *Appl. Phys.* **24** 1134 (1953)
- Stevenson A F J. *Appl. Phys.* **24** 1143 (1953)

74. van Bladel J *IEEE Trans. Microwave Theory Tech.* **23** 199 (1975)
75. Mongia R K, Bhartia P *Int. J. Microwave Millimeter-Wave Comput.-Aided Eng.* **4** 230 (1994)
76. Brillouin L J. *Phys. Radium* **3** 373 (1932) <https://doi.org/10.1051/jphysrad:0193200309037300>
77. Muljarov E A, Langbein W, Zimmermann R *Europhys. Lett.* **92** 50010 (2010)
78. COMSOL, <https://www.comsol.ru/>
79. Electromagnetic Systems Modeling. CST Studio Suite. Dassault Systèmes, <https://www.3ds.com/products-services/simulia/products/cst-studio-suite/electromagnetic-systems/>
80. Bai Q et al. *Opt. Express* **21** 27371 (2013)
81. Yan W, Faggiani R, Lalanne P *Phys. Rev. B* **97** 205422 (2018)
82. Mie G *Ann. Physik* **25** 377 (1908) by new numbering Vol. 330
83. Luk'yanchuk B S et al. *J. Opt. A* **9** S294 (2007)
84. Tribelsky M I, Luk'yanchuk B S *Phys. Rev. Lett.* **97** 263902 (2006)
85. Tribelsky M I, Miroschnichenko A E *Phys. Usp.* **65** 40 (2022); *Usp. Fiz. Nauk* **192** 45 (2022)
86. Bashevoy M V, Fedotov V A, Zheludev N I *Opt. Express* **13** 8372 (2005)
87. Noh H et al. *Phys. Rev. Lett.* **108** 186805 (2012)
88. Proskurin A, Bogdanov A, Baranov D *Laser Photon. Rev.* **15** 2000430 (2021)
89. Smythe W R *Static and Dynamic Electricity* 3rd ed. (New York: McGraw-Hill, 1968); Translated into Russian: *Elektrostatika i Elektrodinamika* (Moscow: IL, 1954)
90. Guzatov D V, Klimov V V, Pikhota M *Laser Phys.* **20** 85 (2010)
91. Guzatov D V, Klimov V V *Chem. Phys. Lett.* **412** 341 (2005)
92. Hobson E W *The Theory of Spherical and Ellipsoidal Harmonics* (Cambridge: The Univ. Press, 1931)
93. Faggiani R et al. *ACS Photon.* **4** 897 (2017)
94. Mårzell E et al. *Nano Lett.* **15** 6601 (2015)
95. Klimov V V, Guzatov D V *Phys. Rev. B* **75** 024303 (2007)
96. Klimov V V *Phys. Usp.* **51** 839 (2008); *Usp. Fiz. Nauk* **178** 875 (2008)
97. Klimov V V, Guzatov D V *Appl. Phys. A* **89** 305 (2007)
98. Nordlander P et al. *Nano Lett.* **4** 899 (2004)
99. Prodan E, Nordlander P *J. Chem. Phys.* **120** 5444 (2004)
100. Guzatov D V, Klimov V V *New J. Phys.* **13** 053034 (2011)
101. Watson J D et al. *Molecular Biology of the Gene* 7th ed. (Boston: Pearson, 2014)
102. Pal S et al. *Angew. Chem.* **122** 2760 (2010); *Angew. Chem. Int. Ed.* **49** 2700 (2010)
103. Zheng J et al. *Nano Lett.* **6** 1502 (2006)
104. Kuzyk A et al. *Nature* **483** 311 (2012)
105. Mastroianni A J, Claridge S A, Alivisatos A P *J. Am. Chem. Soc.* **131** 8455 (2009)
106. Klein W P et al. *Nano Lett.* **13** 3850 (2013)
107. Ding B et al. *J. Am. Chem. Soc.* **132** 3248 (2010)
108. Roller E-M et al. *Nano Lett.* **15** 1368 (2015)
109. Roller E-M et al. *Nat. Phys.* **13** 761 (2017)
110. Klimov V V, Sharonov G V *Quantum Electron.* **50** 237 (2020); *Kvantovaya Elektron.* **50** 237 (2020)
111. Many V et al. *Nanophotonics* **8** 549 (2019)
112. Il'chenko M E et al. *Dielektricheskie Rezonatory* (Dielectric Resonators) (Ed. M E Il'chenko) (Moscow: Radio i Svyaz', 1989)
113. Luk K M, Leung K W (Eds) *Dielectric Resonator Antennas* (Antennas Series) 1st ed. (Baldock: Research Studies Press Ltd, 2002)
114. Vahala K *Nature* **424** 839 (2003)
115. Kuznetsov A I et al. *Science* **354** aag2472 (2016)
116. Sager O, Tisi F *Proc. IEEE* **56** 1593 (1968)
117. Gastine M, Courtois L, Dormann J L *IEEE Trans. Microwave Theory Tech.* **15** 694 (1967)
118. Martin R J, Tatam R P J. *Mod. Opt.* **41** 1445 (1994)
119. Filonov D S et al. *Appl. Phys. Lett.* **100** 201113 (2012)
120. Kuznetsov A I et al. *Sci. Rep.* **2** 492 (2012)
121. Voshchinnikov N V, Farafonov V G *Astrophys. Space Sci.* **204** 19 (1993)
122. Komarov I V, Ponomarev L I, Slavyanov S Yu *Sferoidal'nye i Kulonovskie Sferoidal'nye Funktsii* (Spheroidal and Coulomb Spheroidal Functions) (Moscow: Nauka, 1976)
123. Lai H M et al. *J. Opt. Soc. Am. B* **8** 1962 (1991)
124. Luk'yanchuk B S et al. *ACS Photon.* **2** 993 (2015)
125. Bulgakov E, Pichugin K, Sadreev A *Phys. Rev. A* **104** 053507 (2021); arXiv:2107.13719
126. Kishk A, Glisson A W, Junker G P *PIER* **33** 97 (2001) <http://dx.doi.org/10.2528/PIER00122803>
127. Bulygin V S et al. "Axially symmetric modeling of dielectric pillbox resonators", in *2012 14th Intern. Conf. on Transparent Optical Networks, ICTON* (Piscataway, NJ: IEEE, 2012) Tu.B6.3, <https://doi.org/10.1109/ICTON.2012.6253729>
128. Rybin M V, Limonov M F *Phys. Usp.* **62** 823 (2019); *Usp. Fiz. Nauk* **189** 881 (2019)
129. Krasikov S et al. *Phys. Rev. Appl.* **15** 024052 (2021)
130. Ruan Z, Fan S *Phys. Rev. Lett.* **105** 013901 (2010)
131. Qian C et al. *Phys. Rev. Lett.* **122** 063901 (2019)
132. Qian C et al. *ACS Photon.* **5** 1506 (2018)
133. Bulgakov E, Pichugin K, Sadreev A *Photonics* **8** 49 (2021)
134. Klimov V V *Phys. Usp.* **62** 1058 (2019); *Usp. Fiz. Nauk* **189** 1131 (2019)
135. Lu Y et al. *Opto-Electron Adv.* **5** 210014 (2022)
136. Veselago V G *Sov. Phys. Usp.* **10** 509 (1968); *Usp. Fiz. Nauk* **92** 517 (1967)
137. Shelby R A, Smith D R, Schultz S *Science* **292** 77 (2001)
138. Shelby R A et al. *Appl. Phys. Lett.* **78** 489 (2001)
139. Remnev M A, Klimov V V *Phys. Usp.* **61** 157 (2018); *Usp. Fiz. Nauk* **188** 169 (2018)
140. Veselago V G *Phys. Usp.* **54** 1161 (2011); *Usp. Fiz. Nauk* **181** 1201 (2011)
141. Kildishev A V, Shalaev V M *Phys. Usp.* **54** 53 (2011); *Usp. Fiz. Nauk* **181** 59 (2011)
142. Klimov V V *Opt. Commun.* **211** 183 (2002)
143. Klimov V V *Phys. Usp.* **64** 990 (2021); *Usp. Fiz. Nauk* **191** 1044 (2021)
144. Klimov V, arXiv:2102.12690
145. Bokut' B V, Serdyukov A N, Fedorov F I *Sov. Phys. Crystallogr.* **15** 871 (1971); *Kristallografiya* **15** 1002 (1970)
146. Lindell I V et al. *Electromagnetic Waves in Chiral and Bi-isotropic Media* (Boston: Artech House, 1994)
147. Pendry J B *Science* **306** 1353 (2004)
148. Zhang S et al. *Phys. Rev. Lett.* **102** 023901 (2009)
149. Dong J et al. *Opt. Express.* **17** 14172 (2009)
150. 'Chiral metamaterials', US 8271241, B2, September 18, 2012
151. 'Chiral metamaterials', US 8,271.241 B2. Google Patents, <http://www.google.ch/patents/US8271241>
152. Wongkasem N, Akyurtlu A, Marx K *PIER* **63** 295 (2006)
153. Klimov V V, Guzatov D V, Ducloy M *Europhys. Lett.* **97** 47004 (2012)
154. Klimov V V, Guzatov D V *Phys. Usp.* **55** 1054 (2012); *Usp. Fiz. Nauk* **182** 1130 (2012)
155. Bohren C F *Chem. Phys. Lett.* **29** 458 (1974)
156. Guzatov D V, Klimov V V *New J. Phys.* **14** 123009 (2012)
157. Klimov V V et al. *Opt. Express* **22** 18564 (2014)
158. Klimov V, Guzatov D, in *Singular and Chiral Nanoplasmonics* (Eds N Zheludev, S Boriskina) (Singapore: Pan Stanford Publ., 2014) p. 121
159. Guzatov D V, Klimov V V *Quantum Electron.* **45** 250 (2015); *Kvantovaya Elektron.* **45** 250 (2015)
160. Guzatov D V et al. *Opt. Express* **25** 6036 (2017)
161. Wu C et al. *Phys. Rev. X* **4** 021015 (2014)
162. Davidovich M V *Phys. Usp.* **62** 1173 (2019); *Usp. Fiz. Nauk* **189** 1249 (2019)
163. Roth J, Dignam M J *J. Opt. Soc. Am.* **63** 308 (1973)
164. Totero Gongora J S et al. *Nat. Commun.* **8** 15535 (2017)
165. Wan M et al. *Appl. Phys. Lett.* **110** 031103 (2017)
166. Schwartz J J, Stavrakis S, Quake S R *Nat. Nanotechnol.* **5** 127 (2010)
167. Staude I et al. *ACS Photon.* **2** 172 (2015)
168. Krasnok A E et al. *Laser Photon. Rev.* **9** 385 (2015)
169. Ee H-S et al. *Nano Lett.* **15** 1759 (2015)
170. Singh M et al. *Nanoscale* **7** 1424 (2015)
171. Caldarola M et al. *Nat. Commun.* **6** 7915 (2015)
172. Szenes A et al. *Sci. Rep.* **7** 13845 (2017)
173. Elshaari A W et al. *Nat. Photon.* **14** 285 (2020)
174. Brongersma M L, Cui Y, Fan S *Nat. Mater.* **13** 451 (2014)
175. Kim S J et al. *Nat. Commun.* **6** 7591 (2015)
176. Sousa-Castillo A et al. *Nano Energy* **37** 118 (2017)

177. Lee K-T et al. *Sci. Rep.* **7** 10640 (2017)
178. Vismara R et al. *Opt. Express* **27** A967 (2019)
179. García-Guirado J et al. *Nano Lett.* **20** 585(2020)
180. Yavas O et al. *Nano Lett.* **17** 4421 (2017)
181. Bontempi N et al. *Nanoscale* **9** 4972 (2017)
182. Yang Y et al. *Nat. Commun.* **16** 5753 (2014)
183. Tittl A et al. *Science* **360** 1105 (2018)
184. Rodionov S A, Remnev M A, Klimov V V *Sens. Bio-Sens. Res.* **22** 100263 (2019)
185. Klimov V V et al. *J. Phys. D* **50** 285101 (2017)
186. Mariani S et al. *Opt. Lett.* **39** 3062 (2014)
187. Kuo P S, Bravo-Abad J, Solomon G S *Nat. Commun.* **5** 3109 (2014)
188. Gigli C et al. *Front. Phys.* **7** 221 (2019)
189. Li G-C et al. *Nat. Commun.* **12** 4326 (2021)
190. Shcherbakov M R et al. *Nano Lett.* **14** 6488 (2014)
191. Grinblat G et al. *Nano Lett.* **16** 4635 (2016)
192. Grinblat G et al. *ACS Nano* **11** 953 (2017)
193. Evlyukhin A B et al. *Nano Lett.* **12** 3749 (2012)
194. Staude I et al. *ACS Nano* **7** 7824 (2013)
195. Tonkaev P et al. *Appl. Phys. Lett.* **118** 091104 (2021)